1918
TALLINNA TEHNIKAÜLIKOOL
TALLINN UNIVERSITY OF TECHNOLOGY

FACULTY OF CHEMICAL AND
MATERIALS TECHNOLOGY
DEPARTMENT OF MATERIALS SCIENCE

# HIGH VACUUM EVAPORATION OF SnS PHOTOABSORBER FILMS

## Master Thesis

**Hrachya Kocharyan**

Supervisors:
Dr. Sergei Bereznev,
Senior Researcher, Dep. of Materials Science;
Dr. Revathi Naidu,
Senior Researcher, Dep. of Materials Science

Materials and Processes of Sustainable Energetics
Tallinn 2016

1918
TALLINNA TEHNIKAÜLIKOOL
TALLINN UNIVERSITY OF TECHNOLOGY

KEEMIA- JA MATERJALITEHNOLOOGIA TEADUSKOND
MATERJALITEADUSE INSTITUUT

# SnS FOTOABSORBERI KIHTIDE VAAKUMAURUSTAMINE

## Magistritöö

**Hrachya Kocharyan**

Juhendajad:
Dr. Sergei Bereznev,
Vanemteadur, Materjaliteaduse Instituut;
Dr. Revathi Naidu,
Vanemteadur, Materjaliteaduse Instituut

Materjalid ja protsessid jätkusuutlikus energeetikas
Tallinn 2016

**Declaration**

Hereby, I declare that this master thesis, my original investigation and achievement, submitted for the Master of Science degree at Tallinn University of Technology, has not been submitted for any academic degree.

Hrachya Kocharyan

# Table of Contents

# ACKNOWLEDGMENTS

This research was carried out at the Department of Materials Science. Author is grateful to the financial support from the institutional research funding IUT19-28 of the Estonian Ministry of Education, Research and ERA.NET RUS PLUS Project Flexapp (ETAG15028) and university base finance B54.

I would like to express my sincere gratitude to my supervisors Dr. Sergei Bereznev and Dr. Revathi Naidu for the continuous support, their patience, motivation, enthusiasm, and immense knowledge. Their guidance helped me in all the time of research and writing of this thesis.

I would like to thank Prof. Andres Öpik, Dr. Malle Krunks and Dr. Marit Kauk-Kuusik for providing an excellent opportunity to carry out my studies and research at the Department of Materials Science, and Prof. Enn Mellikov for his support and encouragement during my Master's course.

I express my gratitude to Dr. Kristi Timmo for highly valuable remarks and suggestions. I would like to thank Dr. Jaan Raudoja, Dr. Olga Volobujeva and PhD students Jelena Maricheva and Nicolae Spalatu for their valuable help and support for my thesis work. In addition, I would like to thank everybody whom I worked with in the Department of Materials Science.

I am grateful to all the people who helped and contribute great ideas and advices, especially my family and close friends during my studies in the field of photovoltaic materials science.

And finally, I am grateful to Armenian community of Estonia and especially Sofia Petrosyan for all the invaluable support and care I was provided with during my studies.

# List of Abbreviations

| | |
|---|---|
| ALD | Atomic layer deposition |
| AZO | Aluminum doped zinc oxide |
| CZTSSe | $Cu_2ZnSn(S,Se)_4$ |
| CBD | Chemical bath deposition |
| DC | Direct current |
| EDX | Energy-dispersive X-ray analysis |
| FF | Fill factor |
| FTO | Fluorine doped tin oxide |
| FWHM | full width at half-maximum |
| HVE | High vacuum evaporation |
| ITO | Indium tin oxide |
| JCPDS | Joint Committee on Powder Diffraction Standards |
| LM | Lattice matched |
| PEC | Photoelectrochemical |
| PLD | Pulsed laser deposition |
| PV | Photovoltaic |
| PVD | Physical vapor deposition |
| QCM | Quartz crystal microbalance |
| RF | Radio frequency |
| RT | Room temperature |
| RTA | Rapid thermal annealing |
| SCE | Saturated calomel electrode |
| SLG | Soda lime glass |
| TCO | Transparent conductive oxide |
| XRD | X-ray diffractometer |
| XPS | X-ray photoelectron spectroscopy |
| ZB | Zinc blende |

# Introduction

Solar cells are considered to be an important energy source for future power supplies [1]. However, the price of electricity produced by PV modules is higher than the price of electricity produced by fossil fuels. In order to reach grid parity, significant reductions in module and installation cost should be achieved. One approach to reduce the module cost is using thin film technology [2].

Most of the modern photovoltaic devices are based on either crystalline or polycrystalline silicon technology. Despite their progress, crystalline silicon is a poor absorber with an absorption coefficient of around $10^2$ $cm^{-1}$ and an indirect band transition of 1.1 eV, which needs more energy to absorb light in solar spectrum. In order to have the superior PV device performance, it requires higher amount of material (hundreds microns thick) [3].

To compete the PV market further in a cost-effective way for electricity generation, the alternative idea is "Thin film technology", which uses materials with high absorption coefficient and suitable band gap, and the key aspect is to use limited amount of material. In thin film solar cells, where the semiconductor film thickness varies from a few hundred nanometers (nm) to tens of micrometers (μm), the typical material usage is about 2-6 $g/m^2$, which decreases the manufacturing cost and makes it viable for economic utilization even for expensive materials. The main difficulty in thin film technology is developing suitable semiconductor devices that have high conversion efficiency and making them cheap in high scale mass-production [2].

The continuous increase of thin film solar cell fabrication as well as potential large scale production in future raised attention towards the concerns of various materials' availability. The most used classic thin film solar cell absorber materials are CdTe, $CuInGaSe_2$ (CIGS) that have reached the laboratory conversion efficiencies of 21.5% [4] and 22.3% [5]. Despite the excellent achievements of CdTe and CIGS, there are concerns like toxicity of Cd, and limited supply of Te, Ga, In, which is the major problem for later developments [6]. One of the most emerging, alternative and new photoabsorber materials is $Cu_2ZnSn(S,Se)_4$ (CZTSSe). CZTS is a quaternary chalcogenide material that was introduced in 1988 by Ito and Nakazawa [7]. CZTSSe has a direct band gap of 1-1.5 eV, high absorption coefficient and good charge mobility; however it is very difficult to control the desired phase composition along with stability [8].

According to Alharbi *et al*. [9], 29 abundant elements form more than a hundred binary and few thousands ternary compounds. They have screened 211 compounds and highlighted 15 most suitable compounds in 5 groups: sulfides (CuS, $Cu_2S$, $FeS_2$, SnS, $WS_2$, $MoS_2$), oxides (CuO), silicides ($\beta$-$FeSi_2$, $\beta$-$BaSi_2$, $Ca_2Si$), nitrides ($\alpha$-$Ca_3N_2$), phosphides ($CuP_2$, $Zn_3P_2$, $\beta$-$ZnP_2$, SiP).

Among the well-known compounds like SnS, $FeS_2$, and $Cu_2S$, SnS attracted much attention as a potential absorber material in photovoltaics with its high absorption coefficient (more than $10^4$ $cm^{-1}$) and suitable direct band gap value (1.3-1.5 eV for single-crystal SnS). Physical investigation of SnS thin films showed sufficient properties to be used as a photoabsorber material in solar cell applications.

However, there are some issues associated with SnS to be used in solar cells e.g. to find optimal conditions in terms of deposition technique and annealing conditions for getting highly photosensitive monophase SnS layers and to eliminate secondary phases, as well as searching suitable alternative buffer layer materials for improving of the photovoltaic properties of the complete solar cell structures.

In this thesis, we are studying SnS thin films deposited onto Mo covered soda lime glass substrates by HVE with following annealing in vacuum at different temperatures to find suitable annealing conditions to obtain single-phase SnS photoabsorber layers. The main novelty of this study is annealing of as-deposited SnS thin films in closed system (sealed ampoules), which is not covered in published works.

**Organization of the Thesis**

- Chapter 1 is describing SnS properties and suitability for PV applications, reviews the history of the development of SnS films and SnS-based solar cells from early crystallography studies to physical vapor deposition techniques for thin film deposition and solar cell preparation.
- Chapter 2 deals with experimental methods used for preparing and investigation of SnS thin films.
- Chapter 3 includes the obtained results, analysis and discussions.
- Chapter 4 represents conclusions from the obtained results.

# Chapter 1: Literature Review

## *1.1 SnS Photoabsorber*

### 1.1.1 SnS Properties and Photovoltaic Suitability

SnS is a IV–VI group semiconductor with layered orthorhombic structure. In recent decade, SnS has attracted a significant interest as an absorber material for photovoltaic cells because:

- It is a simple binary material
- It has a suitable direct and indirect energy band gaps of 1.3-1.5 eV and 1.0-1.1 eV, respectively [10]
- SnS has high optical absorption coefficient, $\alpha > 10^4$ $cm^{-1}$ [6]
- SnS consists of less toxic and earth abundant elements [6, 9]
- SnS can be fabricated by low-cost deposition technologies (e.g. CBD)

SnS is an intrinsic p-type semiconductor with a hole concentration of $10^{16}$-$10^{18}$ $cm^{-3}$ and Hall mobility around 90 $cm^2/Vs$ at room temperature. Optimal band gap and electron affinity ($E_g$ = 1.3 eV and $\chi$=4.2 eV) makes SnS suitable for integration with n-type buffer layer with similar electron affinity along with wider band gap [11]. The static dielectric constant and refractive index of SnS crystals are 12.41 and 3.52, respectively [12].

### 1.1.2 Earth Abundance and Environmental Impacts of SnS

In last decades, intensified efforts were made to improve the efficiency of thin film solar cells despite the price of the final product and materials used in it. This pursuit for record efficiency material found that GaAs (gallium arsenide) demonstrated the highest solar cell efficiency of 28.8% [13, 14], which consists of expensive gallium and highly toxic arsenium. Both these elements can limit future commercial use of gallium arsenide based solar cells. According to numerous studies, in contrast, SnS can be a good candidate to become a commercially used large-scale material for solar cells due to its promising technical properties. As illustrated in the *Figure 1*, both sulfur and tin are widely available elements in the earth crust. For instance, sulfur is in orders of magnitude more abundant than copper and/or lead, so it will not become an endangered element in the near future. As it can be seen from the *Figure 1*, tin is less earth-abundant than sulfur, however tin is broadly available across geo-political boundaries, which make it more robust to political and economical

changes. Also, tin is a much more abundant material than a number of other photovoltaic elements e.g. cadmium or tellurium [15].

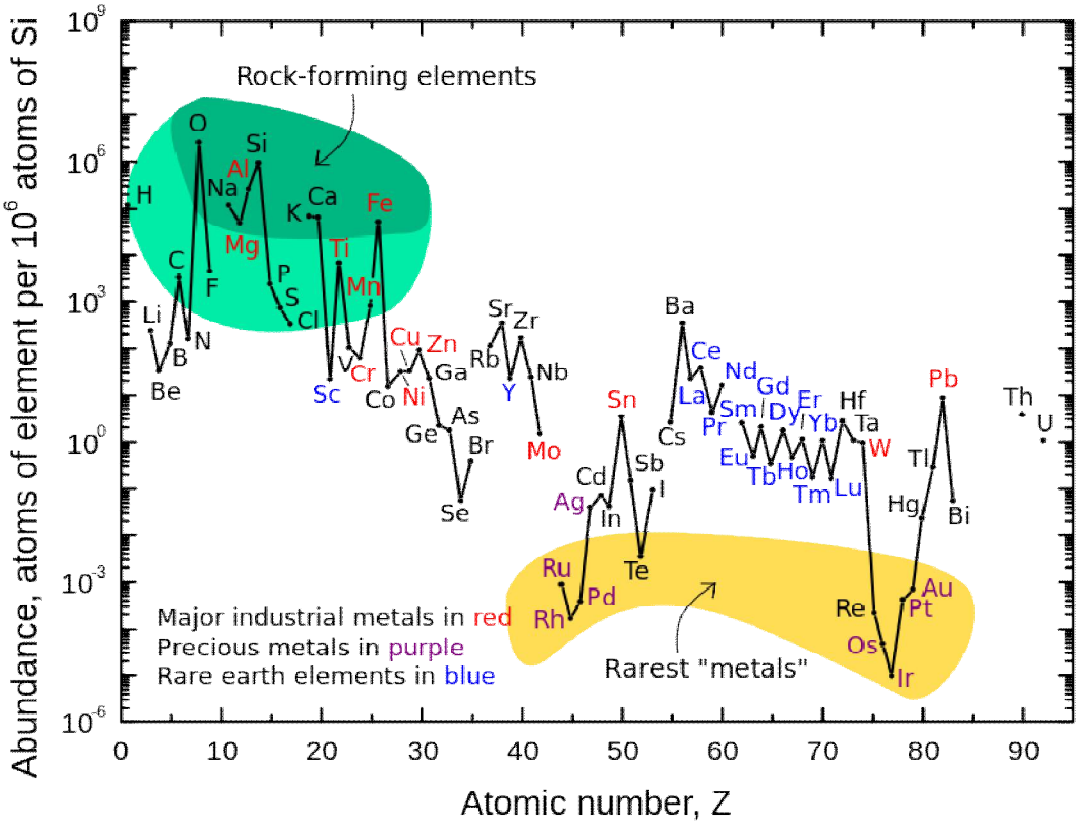


*Figure 1: Abundance of elements in the earth's crust relative to silicon as a function of atomic number.* [15]

Burton [16] calculated total SnS material use in solar cells to cover global energy demand as of 2011. Taking into account a hypothetical l5 µm thick SnS films and 10 % efficient solar cell, he estimated the total use of SnS to be $3.233\times10^6$ kg, from which tin is $2.545\times10^6$ kg, whereas in 2014, world tin reserves were estimated to be $4.8\times10^9$ kg [17], which means that resources of tin are 3 orders of magnitude more than required amount of tin to support world energy needs.

## *1.2 SnS Crystal Structure*

Tin monosulfide is a IV-VI group of compound semiconductor [18]. SnS (herzenbergite) was discovered by Prof. Robert Herzenberg in 1934 in the Maria-Teresa mine near Huari, between Oruro and Uyuni, Bolivia [19].

Tin monosulfide crystals predominantly exhibit orthorhombic structure (Pnma-B16 2h space group) with lattice parameters $a$=3.98 Å, $b$=4.33 Å, $c$=11.18 Å through four molecules in the unit cell. This structure, which may be described as pseudo-tetragonal, has every 'Sn' atom surrounded by six 'S' atoms, three at a shorter distance (~2.68 Å) with the interatomic directions at angles 88º10′, 88º10′ and 95º8′, respectively, and three atoms at a longer distance (~3.88 Å) with the interatomic directions at angles 118º, 118º and 75º respectively. The first group of 'S' atoms establishes short Sn-S bonds within the layer whereas the second group of 'S' atoms connects two neighboring SnS layers. The interatomic distances of the second group of 'S' atoms form an angle of 78º with the interatomic directions of the first group of 'S' atoms [20].

According to Albers *et al*. [21], the bonding type of SnS apart from its ionic part, is covalent of the $p^3$ type. *Figure 2* shows that SnS has a layer structure with double layers perpendicular to the *c-axis*.

Feng Ke *et al*. [22] investigated the electrical transport behavior of SnS under high pressure and the temperature dependent electrical studies performed by Hall Effect measurements. They observed a semiconductor-semimetal transition at ~10.3 GPa. Moreover, they observed a significant change in the electrical resistivity, carrier concentration, and carrier mobility at 12.6 GPa, which was attributed to be a result of structural phase transition from *Pnma to Cmcm*. According to Chattopadhyay *et al*. [23] the second order phase transition from $\alpha$-phase (*Pbnm-B16*) to the high temperature $\beta$-phase (*Cmcm-B33*) occurs at 887 K (*Figure 2*). This phase transition is caused mainly by the movement of 'Sn' and 'S' atoms along [100] direction.

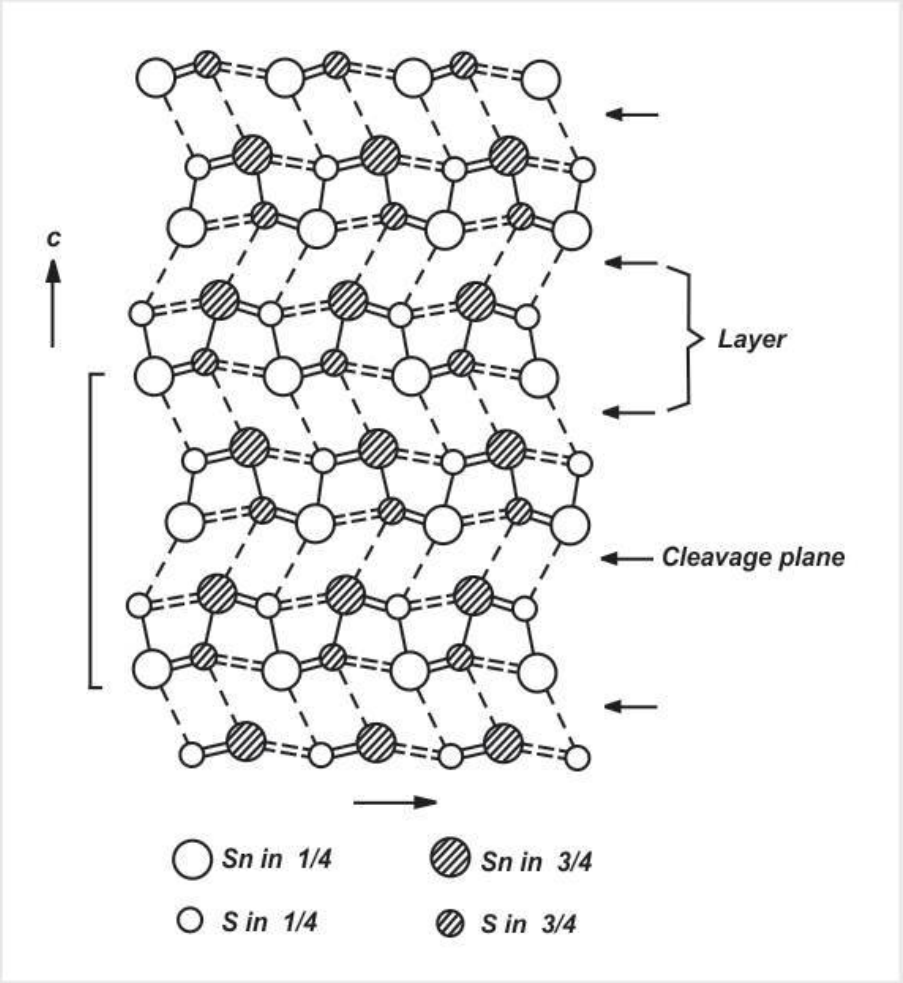


*Figure 2: Orthorhombic crystal structure of SnS. [21]*

Greyson *et al*. [24] describe the synthesis process of zinc blende (ZB) tin sulfide nano- and microcrystals in tetrahedral morphology. According to them, these structures have three-dimensional symmetric shape and exhibit different optical properties than that of orthorhombic structures. From the XRD studies, the evaluated lattice constants were found to be a=b=c=5.845 Å. In order to determine the stability of ZB structure, they examined thermal treatment in dry and wet ambient. While annealing under argon (Ar) at 300ºC for 3h did not change the morphology and crystal structure, annealing in oleylamine at 250ºC for 3h converted the ZB tetrahedra to orthorhombic structure.

Burton and Walsh [25] investigated stability of the different phases of SnS. Besides $\alpha$ and $\beta$ orthorhombic phases, they also examined the existence of zinc blende (ZB) structure and rocksalt structures. In addition to experimental investigation of SnS, they also calculated the formation enthalpies of different phases and explained the stability of different phases from the thermodynamics viewpoint. According to their calculations, the most stable phase is

*α-Pnma* orthorhombic phase. The *β-Cmcm* phase does not form at low temperatures and undergoes a second-order phase transition to the *α-Pnma* phase at 878 K. Based on the calculations, the ZB (*F43m*) phase is not thermodynamically stable and transforms to disordered amorphous phases (*Figure 3e*). In contrast, rock-salt SnS (*Figure 3c*), while it is not the ground-state, it is still thermodynamically stable.

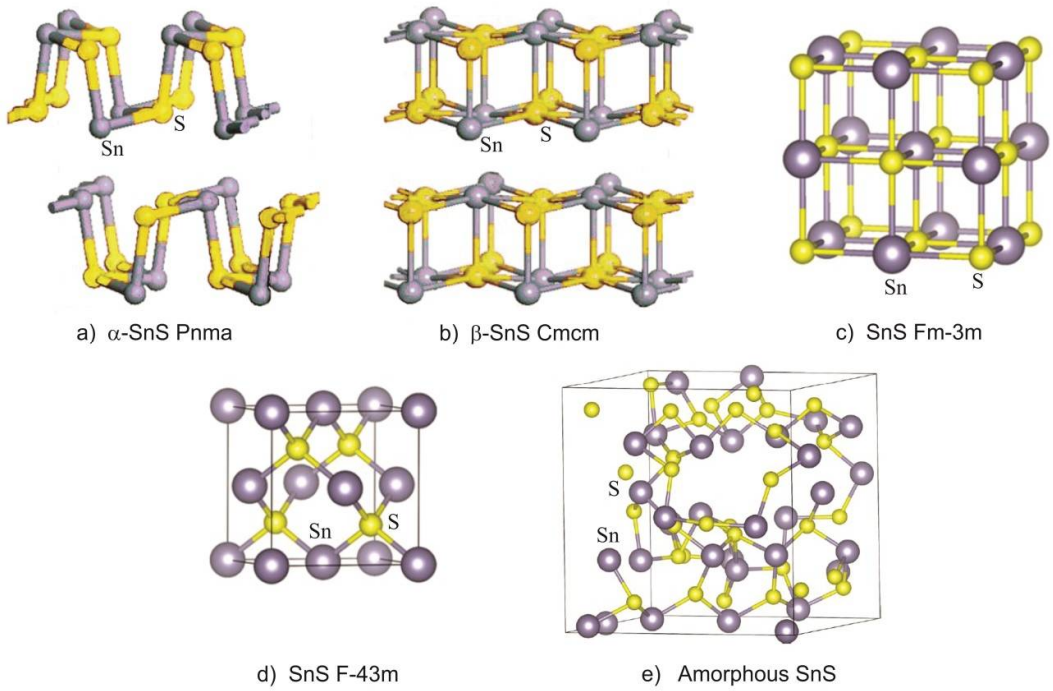


*Figure 3: Different phases of SnS crystal structure: a) & b) polymorphic of orthorhombic c) rock-salt, d) zinc blend, e) amorphous*

## *1.3 Phase Diagram of SnS*

In order to synthesize single crystals, it is necessary to know the phase diagram. Albers *et al.* [26, 27] presented a detailed report on the phase equilibrium of SnS (*Figure 4*). Thermal, chemical and X-ray diffraction methods were used for analyses. They indicated the existence of SnS and $SnS_2$ compounds at melting points of 1153 K and 1143 K, respectively. They state that the boiling point of SnS at normal air pressure is 1503 K. In the temperature interval of 858-875 K the polymorphous transformation was observed. The authors assume the formation of $Sn_2S_3$ and $Sn_3S_4$ by peritectic reaction. At the Sn rich side of the system, in the range of 10-47 at. % S, there is a monotectic region at 1133 K, where solid SnS, a liquid

phase having a composition close to SnS, Sn rich second liquid phase and a vapor phase are in equilibrium. The second similar domain is observed in the range 70-90 at. % S. The eutectic between SnS and $SnS_2$ is at 1013 K and 55 at. % S.

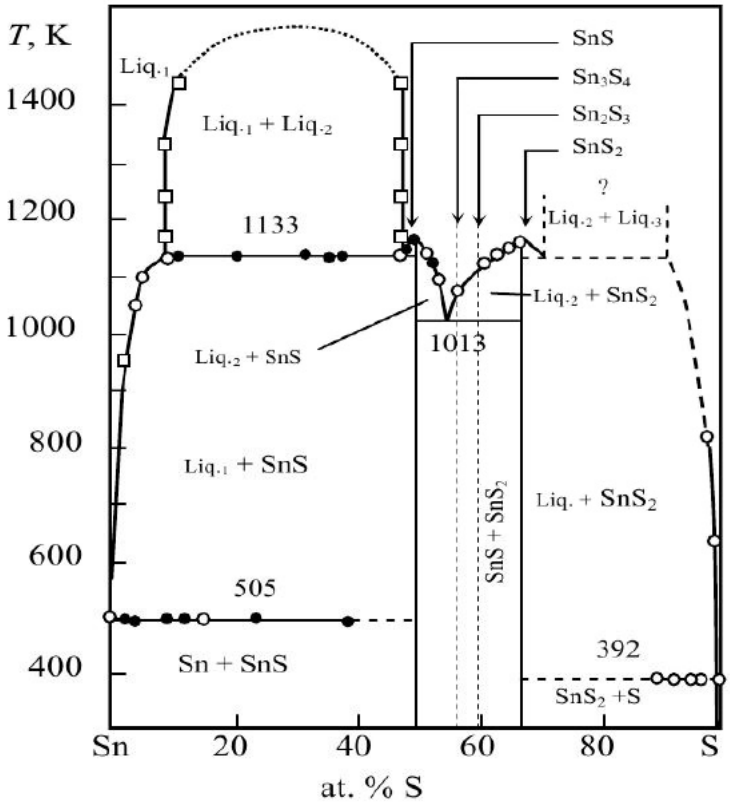


*Figure 4: T-x diagram of SnS*

## *1.4 SnS Crystal Growth*

The pioneering work to grow SnS single crystals was done by Anderson and Morton [28-30]. They used the Bridgemann technique to grow the SnS crystals. Temperature dependent electrical conductivity measurement of SnS was carried out in order to know the electrical properties and the measurements taken from the room temperature to 400ºC and found to fit the expression:

$$\sigma(T) = A_1 e^{\frac{-E_1}{2KT}} + A_2 e^{\frac{-E_2}{2KT}} \quad (1.1)$$

where $A_1$, $E_1$, $A_2$, $E_2$ are constants that characterize the conductivity and can be correlated directly with small changes in compositional stoichiometry by chemical treatments. $A_1$=1-10, $E_1$=0.1-0.35 eV determines conductivity at lower temperatures, whereas $A_2$=300-1200, $E_1$=~0.6 eV determines the conductivity at higher temperatures. They also examined thermal treatment in hydrogen, oxygen and hydrogen sulfide. The annealing was done at temperatures

up to 350ºC. At temperatures below those where reduction of SnS to metallic tin occurs, they observed that treatment in hydrogen resulted a sharp decrease in conductivity, however, thermal treatments in oxygen and/or hydrogen sulfide showed similar conductivity to as-grown crystals without any significant variations.

Albert and Haas [31] have grown SnS crystals by melting respective elements in a quartz tube at 900ºC. They studied the room temperature electrical and optical properties and determined that the SnS layers had p-type conductivity with a hole concentration of $10^{17}$-$10^{18}$ $cm^{-3}$ and hole mobility of 65 $cm^2/Vs$, respectively. Room temperature Infrared transmission measurements on cleavage plate, perpendicular to the *c-axis* showed the energy band gap values of 1.07±0.04 eV. The absorption curve revealed a square dependence of absorption coefficient from the wavelength - $\alpha \approx \lambda^2$.

## *1.5 Physical Deposition Techniques for SnS Thin Films*

Physical deposition techniques includes high vacuum evaporation (HVE), electron beam evaporation (EB), sputtering, closed space vapor transport (CSVT), atomic layer deposition (ALD), brush plating, hotwall deposition (HWD), pulsed laser deposition (PLD) and molecular beam epitaxy (MBE).

### 1.5.1 High Vacuum Evaporation

High vacuum evaporation (HVE) is a technique used to deposit thin films of various materials inside a vacuum chamber. The deposition is done at low pressure ($10^{-6}$-$10^{-5}$ Torr) to avoid reaction between the vapor and atmosphere. Using resistive heating, the vapor is generated by boiling or subliming the source material. The evaporated material is then transported from the source to the substrate and condensed on the substrate as a solid film. In the HVE method, molecules reaching the substrate material have low energy in order of tenths of eV, which can affect the morphology of the films, often resulting porosity and problems in strength of films' adherence [32].

Noguchi *et al*. [33] were first to describe n-CdS/p-SnS based heterojunction solar cell fabricated by vacuum thermal evaporation. The junction was made in superstrate structure with configuration glass/ITO/n-CdS/p-SnS/Ag. They observed p-type conductivity in as-deposited SnS films with a resistivity of 13-20 Ωcm, with carrier density of $6.3\times10^{14}$-$1.2\times10^{15}$

$cm^{-3}$ and a Hall mobility of 400-500 $cm^2/Vs$. They used a substrate temperature in the range of 150-350 ºC and observed a change in the most prominent peak in XRD from (111) to (040) with an increase of substrate temperature. They obtained a direct band gap of 1.48 eV and absorption coefficient of films was in order of $10^4$ $cm^{-1}$ at the fundamental absorption edge. They reported a short-circuit current of 7 $mA/cm^2$, an open-circuit voltage of 0.12 V, a fill factor of 0.35, and a conversion efficiency of 0.29 %.

Devika *et al*. [11] describe deposition of 4N pure SnS films onto Corning 7059 glass using high vacuum evaporation technique. They deposited 0.5 μm thick films with the rate of deposition of 10 Å/s and at different substrate temperatures varying from room temperature to 325 ºC. They observed loss of sulfur in the layers with increase of the substrate temperature. At low temperatures they observed Sn/S ratio of 0.87. With increase of the substrate temperature, they obtained a near stoichiometric composition at about 225 ºC. This change in composition might be caused by re-evaporation of sulfur. At substrate temperatures less than 125ºC they observed dominant SnS phase with additional $SnS_2$ and $Sn_2S_3$ phases. At the temperatures between 125 ºC and 275 ºC the films contained mainly SnS and $Sn_2S_3$ phases with different orientations. At the temperatures higher than 275 ºC, the films contained only SnS phase with different orientations. According to the XRD data, the intensity of SnS phase along (111) direction was maximum at temperature of 275 ºC. With the increase of the temperature, the films conductivity slowly increased up to 175 ºC, and sharp increase at higher temperatures. For the films deposited at the temperatures higher than 225 ºC, an average conductivity was $3.12\times10^{-2}$ $\Omega^{-1}cm^{-1}$. They observed high energy band gap of 1.65 eV at low temperatures, and at higher temperatures the band gap was around 1.33-1.35 eV.

Ogah *et al*. [34] have studied vacuum evaporation of 4N pure SnS onto soda-lime glass. Films were deposited using source temperature in the range of 300-600 ºC and substrate temperatures in the range of 100-400 ºC. Deposited films were adherent to the substrate, uniformly thick and pinhole free. The films with less than 4 μm thickness had smooth surface topology and yellow-brown color, whereas films with more than 10 μm thickness had rougher surface and darker color. They observed decrease of tin concentration with increasing substrate temperature from 100 ºC to 300 ºC and at source temperature of 300 ºC. At substrate temperature of 300 ºC, and the source temperature changing between 300 ºC and 500 ºC, they observed increase of tin concentration. They observed band gap energy more than 1.9 eV for film thickness less than 0.6 μm deposited at constant source and substrate temperatures. The band gap was decreased with increasing thickness. For film thickness of 3 μm, deposited at

source temperature of 300 ºC and with the substrate temperature in between 280-350 ºC, the band gap was 1.4-1.7 eV.

Reddy [35] has reported the influence of growth-temperature on the morphology and orientation of SnS thin films deposited by vacuum evaporation. The films were deposited at three temperatures: 275, 300 and 350 ºC with 0.2 nm/s deposition rate and with a thickness of 200 nm onto glass substrates. All samples were pinhole free, and the adhesion of the films with the substrate was increased with increase of the temperature. Films grown at 300 ºC had the lowest surface roughness. With increasing growth temperature films became tin rich, since the Sn/S ratio increased from 0.988 to 1.105, which may be resulted by scattering loss of sulfur. Crystals of films deposited at 275 ºC had orientation along the (111) direction, while films deposited at 300 ºC had crystals oriented along either (111) or (040) and films deposited at 350 ºC had crystals oriented at (040). With increasing temperature they observed exponential decrease of '*a-axis*' and increase of '*c-axis*' lattice parameters, whereas the lattice parameter '*b*' increased linearly. While increasing the substrate temperature from 275 ºC to 350 ºC, the resistivity of the films decreased from 335 Ωcm to 97 Ωcm. The direct band gap of the films deposited at 275 ºC was 2.01 eV, and it decreased to 1.91 eV for films deposited at 350 ºC.

Schneikart *et al.* [36] studied thermal evaporation of SnS thin films for solar cell preparation. They deposited SnS film onto AZO substrate at a source temperature of 740 ºC. They varied the substrate temperature between 60 and 250 ºC to investigate the influence of temperature on the morphology, structure and compositional properties of SnS films. The deposited films exhibit orthorhombic crystal structure and the crystallinity of the films was increased with increasing temperature to 210 ºC, no change was observed, between 210 and 250 ºC. Films prepared at substrate temperatures up to 210 ºC had flake-shaped grains, whereas film grown at 250 ºC had rectangular grains with an average grain size of 0.9 µm. They observed Sn/S ratio to be between 1.2-1.3 with XPS-measurement, whereas EDX measurements showed an Sn/S ratio of 1.

El-Nahass *et al.* [37] deposited SnS films onto optical flat fused quartz and ordinary glass substrates by thermal evaporation at room temperature. Films were deposited at different film thicknesses varying from 55 nm to 365 nm. They reported, the chemical composition to be Sn-50.05 at.% and S-49.95 at.%. The as-deposited films were amorphous with a wide XRD peak around 23°. For all thicknesses, the reflectance and transmittance studies showed that both parameters increased with increasing wavelength up to 575 nm and the sum was less than 1, indicating absorption. For a given wavelength, decrease of both the reflectance and

transmittance was noticed with increase of the thickness. In the range of 575-1250 nm, transmittance increased and reflectance decreased and their sum was less than 1. At wavelengths more than 1250 nm, transmittance increased and reflectance decreased and the sum was 1. The absorption coefficient was the highest value more than $10^5$ $cm^{-1}$ for wavelengths up to 800 nm. The calculated indirect energy band gap was near 1.4 eV.

Devika *et al*. [38] deposited SnS films onto Corning 7059 glass substrate with thicknesses in the range of 0.1-1.25 $\mu m$ using thermal evaporation. The depositions were carried out at a constant substrate temperature of 300 ºC and with deposition rate of 10 Å/s. The elemental composition of the films varied from Sn=52.4 at.% and S=47.6 at.% for 0.1 μm thickness to Sn=50.05 at.% and S=49.95 at.% for 1.25 μm thickness. The increase of sulfur content in regard to film thickness might be reasoned by high substrate temperature and negative gradient of temperature with increasing film thickness. For films with thickness ≤0.5 μm, the preferred orientation was (111), whereas for films with thickness of 0.75 μm, the preferred orientation was (040). Films with ≥0.75 μm thickness showed presence of both (111) and (040) planes. The average grain size of the films increased from 31 nm for 0.1 μm thick films to 140 nm for 0.5 μm thick films and later decreased to 69 nm for 1.25 μm thickness. Films with thickness <0.5 μm had uniform small crystallites on the surface, while thick films >0.75 μm contained crystallites with complex and multiple structure. Electrical resistivity of SnS films decreased with increase of the thickness from the order of $10^3$ Ωcm for 0.1 μm to the order of $10^1$ Ωcm for 1.25 μm. The rate of decrease of the resistivity below 0.5 μm was about 2300 Ωcm/μm in average, while above 0.5 μm it was around 44.8 Ωcm/μm. The absorption coefficient was the highest for 0.1 μm (>$2\times10^4$ $cm^{-1}$) and decreased with increasing thickness. The energy band gap first decreased from 1.6 eV for 0.1 μm to 1.37 eV for 0.5 μm, then increased to 1.5 eV for 0.75 μm and again decreased slowly with further increase of the thickness.

Cheng and Conibeer [39] investigated the effect of thickness on the growth of SnS films deposited with thicknesses of 20, 40 and 65 nm onto glass substrates by thermal evaporation method. The deposition was carried out at substrate temperature of 200 ºC. With increasing thickness, the color of the film had changed from pale yellow to brown. Films contained mainly SnS phase, but a little amount of $Sn_2S_3$ was also observed. All films showed high reflectance. With increasing film thickness, they observed increase in reflectance and decrease in transmittance, at the wavelengths larger than 900 nm. The films showed direct band gap values of 2.15-2.30 eV as a function of thickness.

Cheng and Zhang [40] prepared SnS films with different thicknesses that varied in the range of 65-580 nm at a substrate temperature of 200 ºC, onto glass substrate by vacuum evaporation. The color of the films changes from brown to dark brown with increasing film thickness. They found increase in grain size and surface roughness with increasing thickness. Moreover, the shapes of the grains are similar and regular for film thicknesses between 185-580 nm, whereas for lower thicknesses the grain shape is different. They observed that crystallites grew preferentially along (111) plane. They reported the highest reflectance of the film with 65 nm thickness, decrease of transmittance and increase of the absorption with increase of the thickness. They observed the direct band gap to be in the range of 1.55-2.28 eV.

Jain and Arun [41] deposited SnS films with varying thickness of 150-900 nm onto glass substrate at room temperature by thermal evaporation. They observed, that films with thickness less than 150 nm are amorphous, and short range ordering among the atoms increases with increase of the film thickness. For film thicknesses ≥480 nm they found films to be oriented along the (040) plane. The Raman measurements showed the presence of $SnS_2$ phase, which may be due to the growing technique and preparation conditions. The ratio of sulfur to tin was found to be ≈0.9 for 600 nm and ≈1.1 for 270 nm and 480 nm. The change in grain morphology depending on the film thickness was noticed. SnS films with thicknesses of 480, 600 and 900 nm, exhibit similar grain morphology and the density is increasing with increasing thickness, whereas for 150 nm thick film grains morphology was different and had aspherical shape. The optical studies showed a direct band gap that varied in the range of 1.8-2.1 eV.

Selim *et al.* [42] deposited SnS films onto glass substrates with different thicknesses in the range of 152-585 nm by thermal evaporation at room temperature. They observed that SnS films with 152 and 225 nm thicknesses were amorphous. Films with 283 and 470 nm thickness had orthorhombic crystalline structure with preferred orientation along the (111) plane. The intensity of the (111) peak increased with increase of film thickness, which indicates improvement in the crystallinity of the films. The compositional ratio of SnS films at a thickness of 585 nm was nearly stoichiometric, whereas thinner films were found to be poor in 'S' and rich in 'Sn'. The obtained absorption coefficient was in the range of $3\times10^3$-$4\times10^4$ $cm^{-1}$ and the energy band gap decrease from 1.68 eV to 1.36 eV with the film thickness increase from 152 nm to 585 nm.

Devika *et al.* [43] investigated the effect of different substrates on the physical properties of SnS thin films by thermal evaporation method. SnS thin films were deposited

onto amorphous Corning 7059 glass, polycrystalline ITO-coated Corning 7059 glass, single crystalline Si wafer and single crystalline Ag-coated Corning 7059 glass. The films were deposited at a constant thickness of 0.5 μm, deposition rate of 10 Å/s and at substrate temperature of 300 ºC. The deposited films were pinhole free, smooth and adherent to the surface. The elemental compositional ratio (Sn/S=1.05) was nearly stoichiometric. The glass/SnS films had (111) as preferred orientation with an average grain size of 168.3 nm. The ITO/SnS films had crystals with (111) plane as preferred peak. The lattice parameters of ITO/SnS films are slightly different from the lattice parameters of the bulk SnS. Particularly the a/c ratio of ITO/SnS was 1.255, whereas for bulk SnS it is 1.085. The average grain size along the (111) direction was 405 nm, whereas the overall average grain size was 220.1 nm. The Si/SnS films exhibited preferred direction of orientation along the (040) direction. The a/c ratio of the lattice was slightly smaller than of the bulk SnS. The average grain size along the (040) plane was 80 nm, while the average grain size of the films in total were 180 nm. The Ag/SnS films showed a good match with the bulk one with an average grain size of 164 nm. Both glass/SnS and Ag/SnS films had similar crystallites, which had densely packed morphology but was grown with different shapes and sizes in different directions. On the other hand, the ITO/SnS films had crystallites grown randomly with irregular shapes and sizes. These crystallites were tightly bonded together forming a strong network. The Si/SnS films had loosely packed network of needle shaped crystallites oriented randomly and having the similar size across the film. The ITO/SnS and Ag/SnS films exhibited low electrical resistivity of $8.9\times10^{-3}$ and 0.26 Ωcm, whereas the same value for the glass/SnS and Si/SnS films were 38.8 and 4.67 Ωcm respectively. The absorption coefficient of glass/SnS, ITO/SnS, Si/SnS and Ag/SnS were found to be $7.92\times10^{4}$ $cm^{-1}$, $4.31\times10^{4}$ $cm^{-1}$, $1.89\times10^{4}$ $cm^{-1}$ and $6.47\times10^{4}$ $cm^{-1}$, respectively. The optical band gap of the films were 1.35, 1.62, 1.55 and 1.86 eV respectively.

Reddy *et al*. [44] compared SnS films grown on lattice matched (LM) Al (100) and amorphous glass substrates by thermal evaporation at thickness of 0.5 μm with constant rate of 2 Å/s and at substrate temperature of 300 ºC. Both films were pinhole free and well adherent to the surface of the substrate. Films grown on LM substrate are smoother and had light gray color, whereas the films grown on amorphous substrate were brown. All SnS films were nearly stoichiometric and slightly tin rich with atomic ratio of Sn/S about 1.06. LM/SnS films had grown the crystallites preferentially oriented along (101) plane, whereas for glass/SnS films (111) plane was the dominant peak. The evaluated average grain sizes were

32 nm for LM/SnS films and 49 nm for glass/SnS films. The energy band gaps of the films grown on glass substrates were found to be 1.92 eV.

#### 1.5.1.1 Summary for HVE SnS Thin Films Review

The investigations on HVE SnS films by various authors reported that the most suitable deposition temperature for near stoichiometric composition of SnS are to be at around 300 ºC [11, 34, 38, 43, 44] and the increase of crystallinity with increasing temperature at more than 275 ºC [11, 35]. Optimal film thicknesses for good adherent, uniform and pinhole free grains are reported to be between 300 and 500 nm [38, 40-42, 44] and the optimal deposition rate to be around 2 Å/s [35, 44]. Most of the results exhibit predominant orientations along (040) and (111) planes with orthorhombic crystal structure and have a direct optical band gap varied from 1.35 eV to 2.28 eV.

### 1.5.2 Co-evaporation

Co-evaporation is a physical deposition method, where different elements are evaporated from different sources. Those elements are heated up until they evaporate or sublimate. Then, the elements are transported to the heated substrate, where they condense to form a thin film of desired materials. To avoid oxidation of the row materials, the deposition is performed under high vacuum [32].

Reddy *et al*. [45] used vacuum co-evaporation technique to deposit SnS films onto Corning 7059 glass at different substrate temperatures varying from room temperature to 300 ºC with 50 ºC intervals, with thickness of 1 μm and deposition rate of 10 Å/s. The deposition was done by thermal evaporation of individual 'Sn' and 'S' elements. Deposited films were well adherent to the substrate surface, and the adherence was increased with increase of substrate temperature. At room temperature the color of the films were silver and yellow and changed to grey and brown for higher substrate temperatures. The XRD studies showed various phases of $Sn_2S_3$ and $SnS_2$ at room temperature deposited SnS films. The films deposited at 50 ºC< $T_s$<150 ºC, the main phases were SnS and $SnS_2$ with minor phase of $Sn_2S_3$. With increasing substrate temperature, the intensity of SnS phase along (040) plane increased and reached maximum at 300 ºC, while other phases of SnS, $SnS_2$ and $Sn_2S_3$ decreased with increasing substrate temperature. The average grain size of the films increased from 50 nm to 90 nm with increasing substrate temperature. The electrical resistivity of the

films was found to vary from 6.1 Ωcm to 1.3 Ωcm as a function of substrate temperature. All films exhibited high absorption coefficient of $>10^4$ $cm^{-1}$ and optical energy band gap values vary in the range of 1.27-1.45 eV. SnS films showed the best crystalline structure deposited at 300 ºC and the same films were thermal treated in vacuum ambient at 200 ºC for 3h for getting single phase SnS and better crystallinity. Annealing results in tin monosulfide phase and moreover, other phases were eliminated and had an electrical resistivity of 6.1 Ωcm. These annealed layers are potentially suitable for fabrication of heterojunction device.

Cifuentes *et al*. [46] deposited SnS films onto a glass substrate by co-evaporation method. The films were prepared with different varying depositions parameters. In this report, the substrate temperature was varied from 200 ºC to 400 ºC, sulfur evaporation temperature kept in between 150 and 170 ºC, Sn-deposition rate of 0.7-2.5 Å/s and the S/Sn mass ratio in the range of 2-20. The main phases found to be SnS and $SnS_2$, while a minor $Sn_2S_3$ phase was also observed in films prepared at some conditions. They observed that intensity of SnS phase is increasing with increase of substrate temperature as well as with decrease of S/Sn mass ratio. In the reverse case, they observed increase of $SnS_2$ phase concentration. SnS films had orthorhombic structure with (111) plane as dominant orientation, while for $SnS_2$ films exhibit hexagonal crystal with (001) peak. They observed changes in optical transmittance with influence of different deposition parameters. All films had high absorption coefficient- $>10^4$ $cm^{-1}$, refractive index of 2.5-3.9 and optical band gap in the range of 1.3-1.6 eV.

#### 1.5.2.1 Review Summary for Co-evaporated SnS Thin Films

To summing up the review of co-evaporated SnS films, better crystallinity, structure and phase compositions were obtained at higher substrate temperatures in the range of 300-400 ºC, whereas at lower temperatures films had poor crystallinity and mixture of different phases [45, 46].

### 1.5.3 Sputtering

Sputtering is a physical vapor deposition method, where the molecules or atoms of the target material are ejected by energetic bombardment of its surface layers by ions or neutral particles. The source material is placed inside a vacuum chamber containing an inert gas at reduced pressure [32].

Guang-Pu *et al.* [47] deposited SnS films onto microslide glass substrates by RF sputtering. The deposition was carried out under argon gas pressure of $5\times10^{-2}$ Torr with varying substrate temperature between room temperature and 350 ºC and deposition rate in the range of 3-5 Å/s. By changing Sn/S ratio, they observed various changes like occurrence of $SnS_2$ and $Sn_2S_3$ phases. The color of the films had changed from yellow to dark grey as a function of Sn/S ratio. As-deposited SnS films had p-type conductivity with a resistivity of 20 Ωcm as well as direct energy band gap of 1.43-1.46 eV. By doping antimony and annealing at 350-450 ºC, they obtained n-type conductivity with resistivity of 2 Ωcm.

Hartman *et al.* [48] investigated the effect of sputtering conditions on structural, optical and electronic properties of SnS thin film. RF sputtering was done with argon plasma using a magnetron sputtering system. The deposition was performed on soda-lime glass substrates at a substrate temperature of 80 ºC. They deposited four sets of SnS films with different argon pressure from 5 mTorr to 60 mTorr at constant sputter duration of 60 minutes. They observed orthorhombic SnS phase for low pressure, and presence of $Sn_2S_3$ phase for the film deposited at 60 mTorr. The sputtered films were porous with big grain size, although this trend was decreased with increasing argon pressure. With increasing pressure, the film thickness decreased from 1.58 μm to 0.23 μm. While the target stoichiometric ratio of Sn/S was 0.64, but all the films were rich in tin, which might be due to the loss of sulfur during the deposition process. The resistivity of the films increased with increasing pressure, and the SnS film deposited at 60 mTorr had lower resistivity due to the difference in morphology. All films had an absorption coefficient in the range of $10^3$-$10^4$ $cm^{-1}$ with increase in respect to increasing argon pressure. The deposited films had indirect band gaps in the range of 1.08-1.58 eV.

Stadler *et al.* [49] investigated the effects of target-substrate distance and sputter duration on the physical properties of SnS films. Pulsed direct current magnetron sputtering method was used for target-substrate distance investigation, and SnS films were deposited onto boron silicate glass at room temperature and constant argon pressure and RF sputtering was applied to investigate the properties of SnS thin films as a function of sputter duration. They develop a non-contact numerical model for optical and electrical data from UV/Vis/NIR spectroscopy and also they evaluated possible complex optical conductivity parameters and the compared with electrically measured ones. They observed a band gap of 1.88 eV for target-substrate distance deposition for 6.2 cm target-substrate distance and 1.86-1.96 eV band gap for films deposited at 9 cm distance between the target and substrate. They also

observed similar band gap of 1.88 eV for the duration dependence measurements, the film thickness increased with increasing duration.

Banai *et al*. [50] deposited tin sulfide onto silicon nitride coated silicon wafers and glass microscope slides using RF magnetron sputtering. The deposition was carried out at 5-60 mTorr argon pressure with plasma power ranging from 105 W to 155 W. All films were tin rich and the Sn/S ratio for all films was similar. They observed that power had more significant effect on the deposition rate of films deposited at lower pressure. The main phase of deposited films were orthorhombic SnS. Films deposited at high pressures had preferred orientation of (111) plane, while films grown at lower pressures had secondary inclusion of grains at (101) peak. The size and shape of crystallites decrease with increasing pressure, where the sputtering power had no impact. Optical studies of SnS films deposited on glass slides showed a high absorption coefficient of $10^5$-$10^6$ $cm^{-1}$.

#### 1.5.3.1 Summary for Sputtered SnS Thin Films Literature

Using sputtering, authors reported the presence of secondary phases like $SnS_2$,$Sn_2S_3$ in the deposited films and sensitivity of the films depends on Sn/S ratio of the target [47, 48], however, a near stoichiometric composition and orthorhombic SnS can be achieved at lower argon pressures, which on the other hand results porous films [48]. With increasing argon pressure, the porosity of the films decreases, but the thickness of the films also decrease and secondary phases are found [48, 50].

### 1.5.4 Two-Step Process

Reddy *et al*. [51, 52] deposited 0.2 μm thick SnS thin films from high purity tin target by two-step process using DC magnetron sputtering. The metallic 'Sn' layers were deposited onto glass substrates at room temperature and precursor layers were placed in a graphite box in a quartz tube for sulfurization at temperatures in the range of 100-400 ºC for 20 min. All as-grown metallic layers were amorphous and adherent to the substrate surface. Films sulfurized at temperatures below 150 ºC were not sufficient to convert all the metallic Sn layers to SnS. Films sulfurized at temperatures in the range of 150-300 ºC showed presence of different phases like $SnS_2$, $Sn_2S_3$, SnS and elemental Sn and S. At lower temperatures in this range, $SnS_2$ was dominant peak, whereas $Sn_2S_3$ was dominant at higher temperatures. For temperatures higher than 300 ºC, the preferred phase was SnS. With increasing sulfurization

temperature, the intensity of SnS phase increased. At 325 ºC, the preferred orientation was (111). At temperatures higher than 350 ºC more sulfur deficiency can be observed in spite of sulfur excess. This can be a result of re-evaporation of sulfur from the film. Films deposited at 325 ºC had thickness of 400 nm, nearly stoichiometric composition of 50.6 at. % Sn and 49.4 at.% S. All deposited films were porous with smooth, regularly shaped grains of about 100 nm. The single phase films were p-type with electrical resistivity of $1.5\times10^{2}$ Ωcm, a Hall mobility of 10 $cm^2/Vs$, and a net carrier concentration of $4.2\times10^{15}$ $cm^{-3}$. Optical measurements showed absorption coefficient to be more than $10^4$ $cm^{-1}$ and a direct band gap of 1.35 eV.

Jiang *et al*. [53] used two-step process to deposit SnS thin films by magnetron sputtering at room temperature with 200 nm thick precursor tin layers. Later, the metallic tin layers were sulfurized under sulfur atmosphere at 220 ºC for 15, 30, 45 and 60 minutes. After sulfurization, the film thickness increased from initial 200 nm to 420 nm for different annealing durations. With increasing sulfurization time, the surface area and thickness of SnS are increased because more sulfur atoms diffused deeper into Sn films forming SnS. For 15 min sulfurization, they observed only little amount of formed SnS. With increasing sulfurization time, more SnS was formed, and for 60 min sulfurization time all tin was sulfurized. Optical studies showed higher absorption coefficient of more than $5\times10^{4}$ $cm^{-1}$ for all the samples. The energy band gap of the films sulfurized for 15, 30, 45 and 60 min were evaluated to be 0.9 eV, 1.16 eV, 1.22 eV and 1.3 eV, respectively.

Malaquias *et al*. [54] prepared a solar cell with SnS thin films deposited by two-step sputtering process. First, they deposited Mo back contact by DC magnetron sputtering onto soda lime glass. Then, they deposited metallic ‘Sn’ by DC magnetron sputtering; the deposition was done under Ar atmosphere at an operating pressure of $2\times10^{-3}$ mbar. Later, as deposited Sn films were sulfurized under nitrogen and sulfur vapour atmosphere at 300 ºC, 340 ºC, 430 ºC and 520 ºC sulfurization temperatures for 10 min. They observed decrease in Sn content with increasing sulfurization temperature from near stoichiometric Sn/S=0.98 for 300 ºC to Sn/S=0.63 for 430 ºC, which is nearly stoichiometric to $SnS_2$. For higher temperatures presence of $SnS_2$ and $Sn_2S_3$ was observed. Optical studies showed direct allowed and indirect allowed transitions. The indirect energy band gap values were in the range of 1.16-1.17 eV for all samples almost independent from the sulfurization temperature. Except the sample sulfurized at 430 ºC, they observed direct band gap transition that decreases from 1.45 eV to 1.26 eV for sulfurization temperature of 300 ºC to 520 ºC. This may be because the films are formed by mixtures of SnS, $SnS_2$ and $Sn_2S_3$, which have 1.3 eV,

2.2 eV and 1.0 eV direct band gap, respectively. Sample sulfurized at 430 ºC had a direct band gap of 1.57 eV, probably because the sample was a mixture of $SnS_2$ and $Sn_2S_3$. For solar cell, they deposited 50 nm thick CdS layer by chemical bath method and 200 nm thick ZnO:Ga window layer by RF sputtering. I-V measurements showed maximum FF of 34 % and conversion efficiency of 0.17 % for the sample sulfurized at 340 ºC.

Leach *et al*. [55] describe deposition of SnS films onto Mo-coated soda lime glass by two-step process. First, Sn was deposited by DC magnetron sputtering in argon atmosphere at 5 mTorr pressure, later sulfurized at 300-450 ºC for 2 hours in argon atmosphere with 5 % $H_2S$ concentration. They observed SnS films to be pin-hole free, uniform and well adherent to the surface of the substrate. Films grown at lower temperatures contained additional phases of $Sn_2S_3$ and $SnS_2$. With increasing sulfurization temperature, Sn is converted more to SnS and the concentration of other phases is decreased. Also, they sulfurized Sn using elemental S, and found that elemental sulfur can reduce the sulfurization temperature. They obtained decreasing energy band gap with increasing sulfurization temperature in the range of 1.31-1.36 eV.

#### 1.5.4.1 Summary of Two-Step SnS Thin Films

Various authors describe deposition of SnS films by two-step process. All authors [51-55] describe deposition of tin by sputtering with further sulfurization process. In all reports SnS films consisted secondary phases like $Sn_2S_3$ and $SnS_2$, although their concentration were decreased by increasing the sulfurization temperature [51, 54, 55] and sulfurization duration [53].

### 1.5.5 Other Deposition Techniques

Vidal *et al*. [56] deposited SnS films onto fused silica substrates by pulsed laser deposition (PLD) with varying thickness from 200 nm to 400 nm. The deposition was carried using sulfur-rich target (S/Sn=1.5-2.0) in ultra-high vacuum chamber with a pressure of $10^{-9}$ Torr, laser energy density of 1 J/cm$^2$ (KrF 248 nm) operating at 3-10 Hz and substrate temperature varied in the range, 300-500 ºC. SnS films had preferred orientation along the (100) plane. They obtained an indirect band gap of 1.07 eV and p-type conductivity. They claim that carrier density is maximal under the S-rich conditions, and minimal under Sn-rich conditions, and increases with increasing temperature. The measured carrier density was in

the range of $10^{14}$-$10^{17}$ $cm^{-3}$. The lowest hole concentration of $3\times10^{14}$ $cm^{-3}$ was achieved at 500 ºC. Hall mobility were estimated to be in the range of 4-16 $cm^2/Vs$.

Ran *et al*. [57] describe deposition of 150 nm thick SnS films by PLD. The deposition was done on MgO (100) single crystal substrates using incident laser energy of 3 $J/cm^2$ with KrF laser excitation wavelength of 248 nm and with 10 Hz operating frequency in Ar/$H_2S$ ambient (20 % $H_2S$). Substrate temperature was varied from room temperature to 700 ºC. Films grown at ≥400 ºC had orthorhombic crystal structure. At lower temperatures the films contained randomly oriented polycrystals. The deposition rate decreased with increasing substrate temperature above 500 ºC and no film deposition occurred at >600 ºC, which may be a result of re-evaporation of the deposited film. They obtained a low indirect band gap of approximately 0.86 eV.

Tanuševski *et al*. [58] studied the physical properties of SnS thin films deposited by electron beam evaporation onto microscope glass slides. The films were prepared with thickness of 410 and 810 nm and at a temperature of 300 ºC with 3 nm/s deposition rate. They observed (111) as preferred orientation. Films had absorption coefficient of $1.4\times10^4$ $cm^{-1}$ with an indirect band gap energy of 1.23 eV and a direct band gap energy of 1.38 eV, respectively.

Bashkirov *et al*. [59] reported preparation of Mo/p-SnS/n-CdS/ZnO heterojunction solar cell by hot-wall deposition technique. They varied the deposition temperature in the range of 270-350 ºC and deposited thicknesses from 1.5 μm to 5.5 μm. The best solar cell parameters were obtained with 5 μm thick SnS films deposited at 350 ºC having an open circuit voltage of 132 mV, a short circuit current density of 3.68 $mA/cm^2$, fill-factor of 0.29 and efficiency of 0.5 %.

Nozaki *et al*. [60] deposited SnS films onto MgO (001) and glass substrates using molecular beam epitaxy. They obtained a direct band gap values in the range of 1.7-2.0 eV and indirect band gap values in the range of 1.06-1.09 eV. Wang *et al*. [61] also studied the deposition of SnS by molecular beam epitaxy. They deposited SnS onto soda lime glass, GaAs(100) and $SiO_2$. They obtained an indirect energy band gap of 0.99 eV and a direct energy band gap of 1.25 eV and an absorption coefficient of $10^4$ $cm^{-1}$.

Yanuar *et al*. [62] describe deposition of SnS films by closed-space vapor transport method. They deposited SnS films onto soda lime glass and $SnO_2$ coated soda lime glass substrates at substrate temperatures of 500 ºC and 550 ºC, respectively. They obtained direct energy band gap in the range of 1.28-1.32 eV and absorption coefficient in the order of $10^4$ $cm^{-1}$.

Kim *et al*. [63] describe deposition of thin films of SnS onto $Al_2O_3$ by atomic layer deposition. The deposition was done using tin(II) 2,4-pentanedionate ($Sn(acac)_2$) and hydrogen sulfide ($H_2S$) at different substrate temperatures from 125 ºC to 225 ºC. They obtained high energy band gap of 1.87 eV, which may be a result of oxygen impurities.

Sinsermsuksakul *et al*. [64] deposited SnS films by atomic layer deposition using bis(N,N′- diisopropylacetamidinato)tin(II) [$Sn(MeC(N\text{-}iPr)_2)_2$] and hydrogen sulfide ($H_2S$) at different temperatures that varies from 100 ºC to 200 ºC. They obtained p-type conductivity with a direct energy band gap of 1.3 eV, absorption coefficient of $>10^4$ $cm^{-1}$, carrier concentration of $10^{16}$ $cm^{-3}$ and hole mobility 0.82-15.3 $cm^2/Vs$.

#### 1.5.5.1 Summary of Other Deposition Techniques

Authors mention other techniques e.g. PLD, electron beam evaporation, molecular beam epitaxy, closed-space vapor transport, ALD used to deposit SnS thin films. All authors obtained p-type conductivity and a direct band gap between 1.25 eV and 1.87 eV. From the mentioned deposition techniques, the highest efficiency for SnS based solar cells was achieved using ALD technique, which is the most expensive one.

### 1.5.6 Annealing Effect on SnS Structures

Devika *et al*. [65] deposited 4N pure SnS films onto Corning 7059 glass substrate by vacuum evaporation method. The deposition was performed at a substrate temperature of 300 ºC and at 10 $Å s^{-1}$ deposition rate with a thickness of 0.5 μm. The as-deposited films were annealed in vacuum chamber at temperatures of 100, 200, 300 and 400 ºC for 1 h under $10^{-5}$ Torr vacuum. They reported that films were pinhole free, smooth and strongly adherent to the surface of the substrate. They observed Sn/S ratio increase from 1.06 to 1.11 with the increase of annealing temperature. This change in composition might be due to sulfur re-evaporation. SEM studies showed increase in density of crystallites with increase of the annealing temperature. The grain size of the films decreased from 152 nm to 50 nm with increasing annealing temperature. The electrical resistivity was decreased from 37.4 to 9 Ω×cm with increasing annealing temperature this was because the films became more tin rich. The energy band gap of the films first decreased from 1.37 eV to 1.35 eV for as-deposited to films annealed at 100 ºC, and later increased to 1.42 eV for films annealed at 400 ºC.

Yue *et al*. [66] deposited SnS thin films onto ITO substrate from $SnCl_2$ and $Na_2S_2O_3$ by pulse electrodeposition and later the as-deposited films are annealed at 100, 150, 200 and 250 ºC in air for 1 h. They observed that the grain size increases with increase of the annealing temperature. At annealing temperature more than 150 ºC the SnS films started to decompose and were oxidized to $SnO_2$ at 250 ºC. The calculated direct energy band gap values for as-deposited and films annealed at 100 ºC, and 150 ºC were 1.31, 1.37 and 1.39 eV, respectively.

Devika *et al*. [67] investigated the effect of rapid thermal annealing (RTA) on SnS films. They deposited 0.5 µm thick SnS films onto Corning 7059 glass substrates by thermal evaporation at a substrate temperature of 300 ºC with 2 Å/s deposition rate. As-deposited films were annealed using RTA technique at temperatures from 300ºC to 550 ºC in nitrogen atmosphere for 1 min. All films were pinhole free, smooth and adherent to the surface of the substrate except films annealed at 550 ºC. At 550 ºC they observed removal of some SnS layers. With increasing temperature, they observed decrease in sulfur content, which might be a result of sulfur re-evaporation from the films. They observed p-type conductivity in all films and the resistivity of the films decreased from 28 Ωcm to 5 Ωcm for films annealed at 400 ºC, above which it increased slightly. The Hall mobility of the carriers increased from 5 $cm^2/Vs$ to 99 $cm^2/Vs$ with increasing annealing temperature up to 400 ºC, and decreased above this temperature. Depending on the annealing temperature, the concentration of carriers changed in the range of 1.1-1.5 × $10^{16}$ $cm^{-3}$. This results show that it is possible to obtain a low resistivity SnS films with RTA technique.

Ogah *et al*. [68] thermally evaporated SnS films onto soda lime glass and CdS/ITO glass substrates at different substrate temperatures varied in the range 100-400 ºC and then annealed in vacuum at temperatures from 300 ºC to 500 ºC for different durations (15 minutes to 3 hours). For all the samples they found mainly SnS phase with presence of $SnS_2$ and $Sn_2S_3$ phases. They observed densification and increase in grain size with increasing annealing temperature and duration.

Jia *et al*. [69] deposited SnS and Ag films onto glass substrates by vacuum thermal evaporation and then annealed at 210, 260 and 300 ºC temperatures in nitrogen atmosphere for 2 h to obtain silver doped SnS films. They obtained improvement in crystalline structure after annealing, with preferred orientation of (111) plane. They observed high absorption coefficient greater than $1.3\times10^5$ $cm^{-1}$ for all films. The absorption coefficient increased with increasing annealing temperature, which might be a result of improved crystallization. The estimated energy band gap was 1.3 eV. With increasing annealing temperature, they observed

increase in carrier concentration and mobility values that reaches to the maximum of $1.132\times10^{17}$ $cm^{-3}$ and 17.8 $cm^2/Vs$, respectively.

Devika *et al*. [70] deposited 50 nm thick SnS films at a substrate temperature of 150 ºC by thermal evaporation and as-deposited films were annealed in nitrogen atmosphere at different temperatures from 100 ºC to 550 ºC for 1 min by RTA technique. Films annealed at temperatures less than 500 ºC were pinhole free, smooth and adherent to the surface. Films annealed at higher temperatures were destroyed due to SnS re-evaporation. They observed crystallites with preferred orientation along the (111) plane. With increasing annealing temperature, increase in tin content was observed. All investigated films had p-type conductivity and with increasing the annealing temperature up to 300 ºC, their resistivity decreased from 43 Ωcm to a minimal value of 36 Ωcm. However, with further increase of the annealing temperature resistivity value increased to 128 Ωcm at 500 ºC. The highest Hall mobility 41 $cm^2/Vs$ was obtained for films annealed at 300 ºC, and the carrier density for all samples was in order of $10^{15}$ $cm^{-3}$. Estimated direct and indirect energy band gap values varied in between 2.09-1.98 eV and 0.48-0.28 eV, respectively.

Ghosh *et al*. [71] deposited 650 nm thick SnS films onto soda lime glass by thermal evaporation at substrate temperature of 250 ºC. As-deposited films were annealed in argon ambient at 200 ºC and 300 ºC for 2, 4 and 6 h along with films that were annealed at 400 ºC for 2 and 4 h. All films consisted of orthorhombic SnS with preferred orientation along the (111) plane. They observed separation of metallic Sn phase from SnS phase at 400 ºC, which might be due to re-evaporation of sulfur. Following this, the Sn/S atomic ratio changed from 0.97 to 2.92 as a function of annealing temperature up to 400 ºC for 4 h. The estimated optical energy band gaps were in the range of 1.33-1.53 eV and were decreasing with increasing annealing temperature. All samples had p-type conductivity. With increasing annealing temperature the bulk resistivity and Hall mobility decreased from 127 Ωcm to 83.2 Ωcm and from 19 $cm^2/Vs$ to 0.8 $cm^2/Vs$, respectively, and the carrier concentration increased from $2.58\times10^{15}$ $cm^{-3}$ to $9\times10^{16}$ $cm^{-3}$.

Jain *et al*. [72] investigated the dependence of the grain size on the band gap of annealed SnS thin films. They used thermal evaporation to deposit SnS films with thicknesses from 270 nm to 900 nm. Later, the films were annealed in vacuum for 30 min at 373 K and 473 K. All the films had orthorhombic structure with (040) as preferred orientation. They observed a sharp increase in grain size from 12 nm to 25 nm with increasing annealing temperature. Improvement in grain size is more expected in thinner films compared to thicker films. They estimated the direct and indirect energy band gap values to be in the range of 2.1-

1.8 eV and 1.8-1.6 eV, respectively, and they report an inverse proportionality between the grain size and the band gap energy.

Patel *et al.* [73] investigated annealing effect on SnS films deposited by spray pyrolysis. They used $SnCl_2 \cdot 2H_20$ and thiourea to deposit SnS films onto heated (375 ºC) glass substrates. As-deposited films were annealed in argon ambient at 300, 400 and 500 ºC for 30 min. They observed orthorhombic SnS films with minor presence of $SnS_2$ phase, the concentration of impurity phase decreased with increasing annealing temperature. Upon increasing the annealing temperature, films became denser and rougher. With increasing annealing temperature, the thickness of the film decreased from 0.98 µm to 0.45 µm. Optical measurements revealed that absorption coefficient was in the range of $1.1\text{-}3.5\times10^4$ $cm^{-1}$. The estimated direct energy band gap value increased with increasing annealing temperature from 1.29 eV to 1.35 eV. The calculated electrical resistivity was in the range of $5.7\times10^1\text{-}2.9\times10^5$ Ωcm.

Steinmann *et al.* [74] describe preparation and fabrication of thin films of tin sulfide and solar cell structures. SnS thin films were prepared by thermal evaporation. The device was fabricated onto oxidized Si wafer substrate with Mo back contact, a two-layer Zn(O,S)/ZnO buffer layer, ITO as a transparent electrode and Ag metallization. They deposited 1200 nm thick SnS films at a substrate temperature of 240 ºC with 1 Å/s rate of deposition and applied annealing in 4 % $H_2S$ (96 % $N_2$) ambient at 400 ºC and 28 Torr pressure for 60 minutes. After deposition of SnS, they grew a very thin layer of $SnO_2$ (<1 nm) on the surface by leaving the samples in air ambient for 24 hours. They report a huge improvement in grain growth due to annealing in $H_2S$ ambient. They report solar cell parameters to be $V_{OC}$=334.1 mV, $J_{SC}$=20.645 mA/$cm^2$, FF=56.28%, PCE=3.88%.

Sinsermsuksakul *et al.* [75] describe fabrication of SnS solar cells by atomic layer deposition (ALD). The deposition was done on sputtered molybdenum substrate at a temperature of 200 ºC. The SnS thin films were annealed in the deposition chamber with 10 Torr pure $H_2S$ or $N_2$ for 1 h at different temperatures up to 400 ºC. They also formed a thin layer of $SnO_2$ on the surface by leaving the samples in air ambient for 1 day at room temperature, by annealing the samples in 10 Torr of air at 200 ºC for 30 min or by depositing $SnO_2$ using ALD. After, they deposited Zn(O,S) and ZnO by ALD, ITO by RF sputtering and Ni/Al grid lines by electron beam evaporation for final solar cell structure. They reported that annealing in hydrogen sulfide enlarge the crystalline grains and reduce the recombination loss. The recombination is reasoned by sulfur vacancies, which can be reduced by annealing in $H_2S$. They stated that annealing above 500 ºC results a huge mass loss due to SnS re-

evaporation. For films annealed at 400 ºC in nitrogen, they observed slightly increase in grain sizes, while annealing in $H_2S$ resulted in sharp increase in grain sizes. Using films annealed in $H_2S$ at 400 ºC, they prepared solar cells and achieved NREL certified I-V characteristics of $V_{OC}$=372 mV, $J_{SC}$=20.2 mA/cm$^2$, FF=58%, PCE=4.36 %.

#### 1.5.6.1 Summary for Annealing's Literature Review

Authors implemented vacuum annealing mainly using open system (in vacuum chamber and in quartz process tube) [65, 68, 72] and reported that a huge improvement in crystalline structure; however in some cases secondary phases like $SnS_2$ and $Sn_2S_3$ were also found. Annealing in air [66] is not suitable for SnS, since already at as low as 150 ºC SnS starts to decompose and converts to $SnO_2$. Annealing in nitrogen [67, 69, 70] and argon [71, 73] ambient shows improvement in crystallinity, optical and electrical properties, but the improvement is not huge and is less than improvement mentioned in the case of vacuum and $H_2S$ [74, 75] annealing. Majority of the authors report increase in Sn/S ratio with increasing annealing temperature and occurrence of secondary phases like $SnS_2$ and $Sn_2S_3$ as well as decomposition of films was noticed [67, 68, 70, 71, 73, 74]. Various authors report densification and improvement in crystallites with increasing annealing temperature [65, 66, 68-70, 72, 74, 75]. The maximal temperature of annealing in nitrogen ambient, above which the films start to decompose is reported to be around 500 ºC [67, 70, 74].

## *1.6 Scope of the Present Work*

Based on the literature review, it is clear that SnS is relatively new absorber material for solar cell applications and has big potential due to its promising properties like high absorption coefficient of more than $10^4$ cm$^{-1}$ with a suitable band gap of 1.35 eV and p-type conductivity. In recent years, thin films of SnS photoabsorber has been prepared by different methods and physical properties were investigated using various techniques and relatively much work has done on thermal treatments of SnS thin films and their characterization. Several reports showed the presence of $SnS_2$ and $Sn_2S_3$ along with stable SnS phase, but for good solar cells the problem of impurity phases needs to be solved. Moreover, optimal film annealing conditions are not yet investigated and determined completely and no groups were reported the properties of SnS thin films as a function of vacuum annealing using closed system (small ampoules). Therefore, in the present thesis, we make an effort to study the

influence of vacuum annealing of as-grown SnS thin films in closed system to see the changes in their phase composition, structural, morphological, optical properties and photosensitivity and also to develop single-phase SnS photoabsorber layers with annealing for the fabrication of solar cells. It should be noted, that most of published papers have been devoted to studies of SnS layers deposited onto the glass and glass/TCO substrates. In our work, we use mainly glass/Mo substrates as appropriate basis for complete solar cell preparation.

## *1.7 Aim of the Study*

The present investigation is aimed with following objectives that include:

- To deposit SnS thin film by high vacuum evaporation method onto Mo-covered SLG substrates, as well as study the peculiarities of thermal treated as-grown films in suitable ambient for attaining highly photosensitive single phase SnS photoabsorber layers.
- Characterization of the as-deposited and annealed SnS films to know their compositional, structural, morphological, optical and electrical properties, respectively.

# Chapter 2: Experimental Procedure

## *2.1 Substrate Cleaning*

Substrate cleaning is an important aspect for thin film formations influencing the adhesion, presence or absence of pin holes, porosity, film microstructure, morphology and other mechanical properties. A numerous cleaning procedures are available for removing the contaminates from the substrate surface. In the present work, glass and molybdenum coated soda lime glass were used as substrates for SnS thin film depositions. We employed different cleaning procedures for glass and Mo-coated substrates.

Molybdenum coated soda lime glass substrates were cleaned in an ultrasonic bath for 10 min at 50 ºC in 2 steps - 1) initially in 20% solution of Decon 90 in de-ionized (Millipore) water and 2) in de-ionized (Millipore) water as a final step. After each step the substrates were rinsed with de-ionized (Millipore) water and finally dried under a nitrogen flow.

At the first step of cleaning, the glass substrates were immersed in a hot sulfuric acid for 45 min at 50 °C to remove the surface impurities. Then, the substrates were rinsed with de-ionized (Millipore) water, and cleaned in ultrasonic bath for 10 min in de-ionized (Millipore) water, dried under $N_2$ flow and finally cleaned in Novascan PSD UV-Ozone Cleaning System for 15 min before loading the substrates into the deposition chamber.

## *2.2 SnS Thin Film Deposition by HVE*

In the present study high vacuum evaporation (HVE) method was used for deposition of SnS thin films. Thin films of SnS were deposited onto pre-cleaned soda lime glass (SLG) and Mo-coated substrates by BOC-EDWARDS AUTO-500 System. 4N (99.99 %) pure SnS powder (Sigma-Aldrich) was taken as source material and then placed in a tungsten boat for evaporation. The deposition was performed at a base pressure of around $1 \times 10^{-6}$ Torr with source to substrate distance of 25 cm. The films were deposited onto the rotating substrates at a temperature of 300 ºC with film thickness and rate of deposition of about 500 nm and at 2 Å/s, respectively. The rate of deposition and thickness of the deposited films were determined using the quartz crystal microbalance (QCM) monitor EDWARDS FTM7. All the deposition parameters were taken according to [44].

## *2.3 Thermal Treatment*

In order to improve crystallinity, optical and electrical properties, the as-deposited SnS thin films were annealed in vacuum. Vacuum annealing was done at different temperatures (300 ºC, 450 ºC and 500 ºC) in sealed quartz ampoules with ampoule length of ~10 cm and a diameter of 0.8 cm (closed system). The ampoules were sealed at a pressure of $1 \times 10^{-1}$ Torr.

## *2.4 Investigation of Prepared Films*

As-deposited and annealed SnS thin films were analyzed by different characterization techniques to know the nature and quality of the film. The details of the used characterization techniques are given briefly in this section.

The morphology of prepared SnS films was investigated by high-resolution scanning electron microscopy (HR-SEM, Zeiss ULTRA 55). The working principle of SEM is based on investigation of different electron signals emitted after electron beam collides with the sample. The emission of secondary electrons gives information about the morphology whereas the back scattered electrons provide the data about atomic number of the sample. SEM investigations are done under high vacuum so the electrons will not interact with the media. In addition, the elemental composition of the films was detected using energy dispersive X-ray (EDX) spectroscopy (Zeiss Ultra 55 HR-SEM equipped with Rontec EDX Xflash 3001 detector).

The crystalline structure and quality of as deposited and annealed SnS thin films were characterized by X-ray diffraction (XRD) analysis using Bruker AXS D5005 difractometer equipped with CuKα (λ=0.154 nm) X-ray source (40 kV, 40 mA) in Bragg Brentano geometry. In the XRD measurements, the X-rays are generated by a cathode ray tube, filtered to get a monochromatic radiation, concentrated and directed towards the sample. The interaction of X-rays and the sample produces constructive interference when the Bragg's law is satisfied. By scanning a wide range of angles, all diffraction directions can be determined. Using XRD studies, it is possible to identify the crystalline structure and phases of the material, determining the crystallite sizes and orientations as well as atomic arrangements etc.

The average crystallite size was estimated from the XRD spectra using Debye-Scherrer formula [82]:

$$D = \frac{k\lambda}{\beta \cos\theta} \tag{3.1}$$

where D is the average crystallite size in nanometers (nm), K=0.9 is the shape factor, λ is the wavelength of the x-ray radiation (λ=0.154 nm), β is the full width at half-maximum (FWHM) of the preferred peak in radians (rad), θ is the diffraction angle in degrees (deg).

The interplanar spacing of the diffraction pattern was calculated using the Bragg's law given as [82]:

$$d = \frac{n\lambda}{2\sin\theta} \tag{3.2}$$

where d is the inter planar spacing in nanometers (nm), n=1 is the order of diffraction.

The lattice constants of the experimental films were evaluated using the d-spacing formula for orthorhombic structure [82]:

$$\frac{1}{d^2} = \frac{h^2}{a^2} + \frac{k^2}{b^2} + \frac{l^2}{c^2} \tag{3.3}$$

where h, k, l are Miller indices and a, b, c are lattice constants.

The compositional phase purity of the films was analyzed by Raman Spectroscopy (Horiba LabRam HR spectrometer) using λ=532 nm green laser as an excitation source, which was focused to a 1 μm size spot and the spectral resolution of the system was around 0.5 $cm^{-1}$. Raman spectroscopy is a vibration spectroscopy based on inelastic scattering of monochromatic electromagnetic radiation after interaction with molecules and atoms. Phonons and molecular vibrations in every crystal and molecular structure have specific frequencies, determining which gives a specific fingerprint, from which the molecule can be identified.

Optical transmittance and total reflectance studies were performed by optical spectrophotometery using SLG/SnS films. The basic principle of optical spectrophotometery is that electromagnetic radiation from a source is dispersed and this dispersed light is passed through the sample. Parts of transmitted, reflected and absorbed radiations are studied as a function of incident wavelength with a suitable detecting system. In present study, the measurements were recorded using Agilent Cary5000 UV-VIS-NIR spectrophotometer as a function of wavelength in the range of 300-1500 nm to determine the optical absorption coefficient and energy band gap. The absorption coefficient was calculated from the transmittance data using the equation [83]:

$$\alpha = -\frac{\ln\frac{T}{1-R}}{t} \tag{3.4}$$

where α is the absorption coefficient in $cm^{-1}$, T=T%/100 and R=R%/100 are the absolute values of transmission and reflectance, respectively and t is the thickness of the film in nm.

The optical band gap was estimated from Tauc's equation [83]:

$$(\alpha h\nu) = A\left(h\nu - E_g\right)^n \tag{3.5}$$

where A is a constant, $E_g$ is the energy gap and n=0.5 for allowed direct transition and n=2 for allowed indirect transition. In the case of direct transition, $(\alpha h\nu)^2$ versus hν graph will have a linear region, extrapolation of which to αhν=0 will show the direct band gap. Similarly, indirect band gap can be obtained from $(\alpha h\nu)^{1/2}$ versus hν graph.

In this work, van der Pauw method was used for determining the electrical resistivity of the films and the measurements were done with van der Pauw H-50 using 4 Indium contacts. In order to check the photosensitivity and the type of conductivity of the layers, photo-electrochemical (PEC) measurements were performed by Gamry Reference 3000 Potentiostat/Galvanostat/ZRA in a three electrode cell with a platinum counter electrode and saturated calomel electrode (SCE) as a reference electrode. The measurements were carried out at room temperature in a background 0.1 M $H_2SO_4$ electrolyte solution under the chopped white light with an intensity of 100 $mW/cm^2$.

# Chapter 3: Results and Discussion

## *3.1 Composition and Morphology*

The EDX studies revealed nearly stoichiometric composition for all as-deposited and annealed in vacuum SnS films, as it is illustrated in the Table 1. This means that the SnS transfer from the source (tungsten boat) to the substrates in vacuum chamber was congruent.

Table 1: Composition of as-deposited and vacuum annealed SnS films.

| Sample condition | Sn/S ratio |
|---|---|
| As-deposited | 1.01 |
| Annealed at 300 ºC | 1.04 |
| Annealed at 450 ºC | 1.07 |
| Annealed at 500 ºC | 1.07 |

The morphology of prepared SnS films was examined by HR-SEM. The high resolution surface and cross-section SEM images of as-deposited and vacuum annealed SnS films are shown in *Figure 5 and 6*.

It can be seen from the images that all SnS films are uniform and pinhole free with full coverage of the substrate surface. Surface investigation depicts that as-deposited films (*Figure 5a*) have randomly oriented, flake-shaped grains with number of smaller grains, while vacuum annealing changes in morphology of the as-deposited SnS thin films. With increasing annealing temperature (*Figure 5b, c, d*), significant increase in the size of the grains was noticed at the expense of the smaller grains. Increasing annealing temperature led to denser and closely packed morphology with better orientation (which is shown in part 4.2 Structural Properties) of the grains. At an annealing temperature of 500 ºC, grains reach their equilibrium position with maximal in their sizes and more dense morphology was observed. The cross-sectional images (*Figure 6*) also confirm that the as-deposited and annealed SnS layers are uniform and well-adherent grains onto the used substrate surface. From cross-sectional images, it can be observed that as-deposited films consist of flake-like elongated grains with cone edges are grown on the top surface whereas for films annealed at 500 ºC there is a changeover in shape of the grains to plate-like with more thick and dense morphology, which infers that there is a transition in grain growth from quasi two dimensional towards three dimensional as a function of annealing.

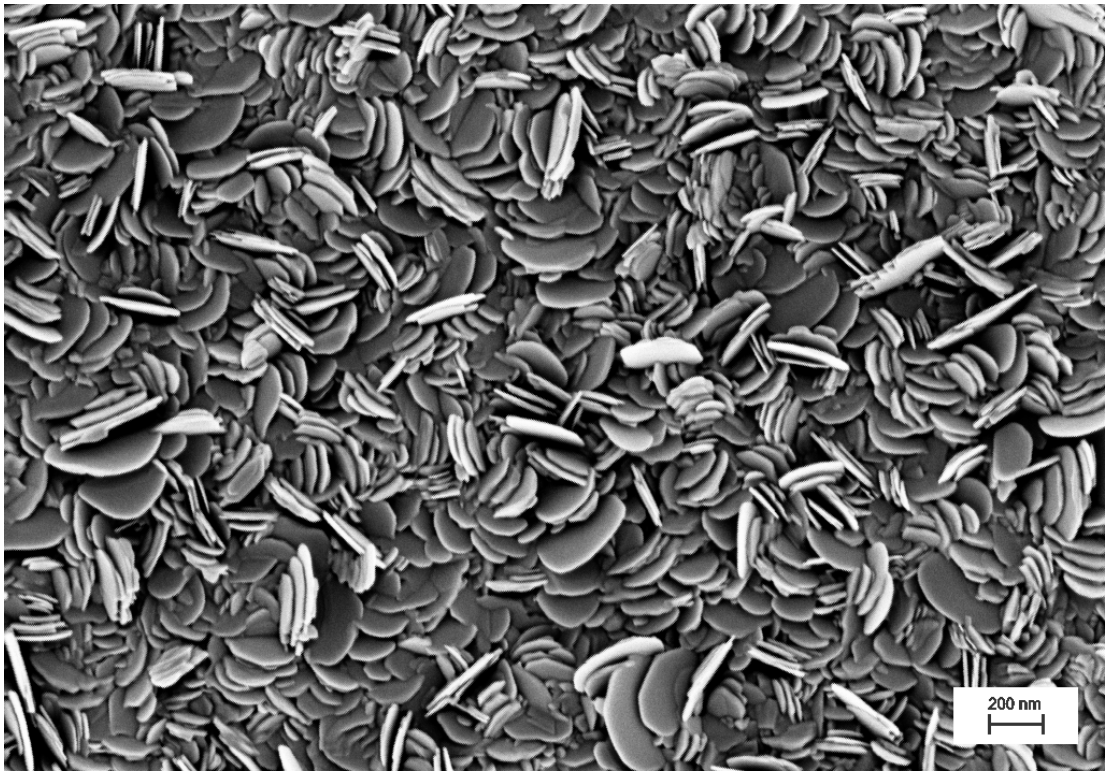


a)

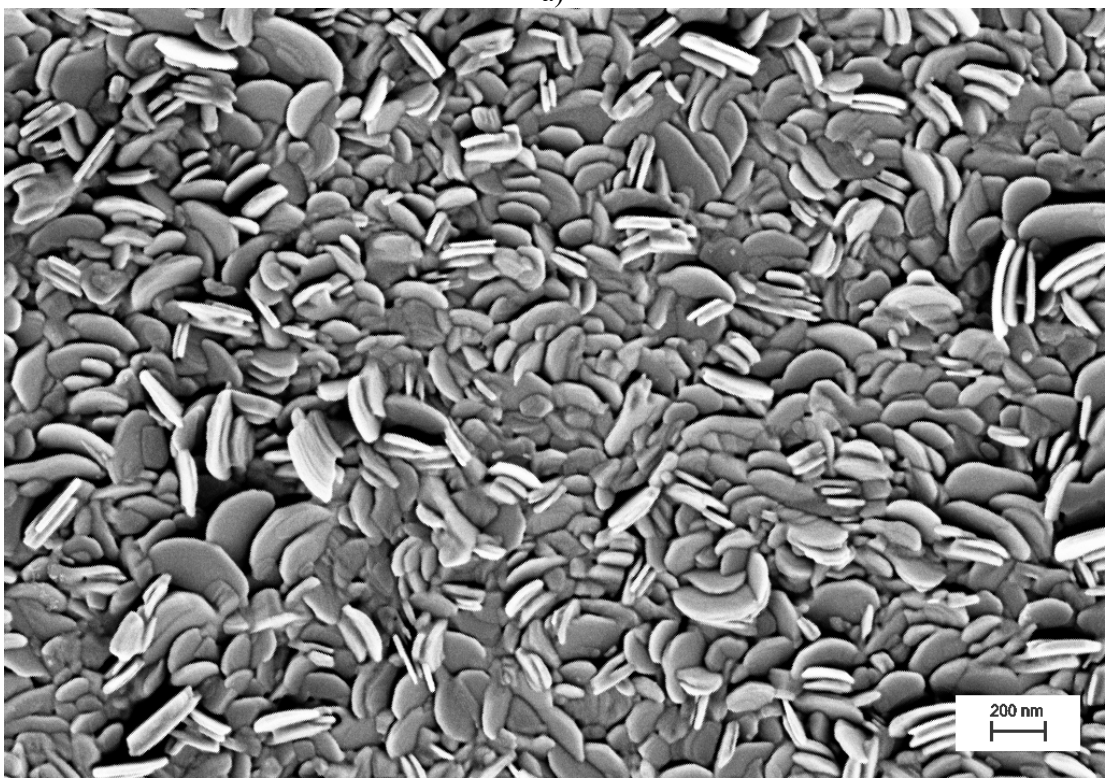


b)

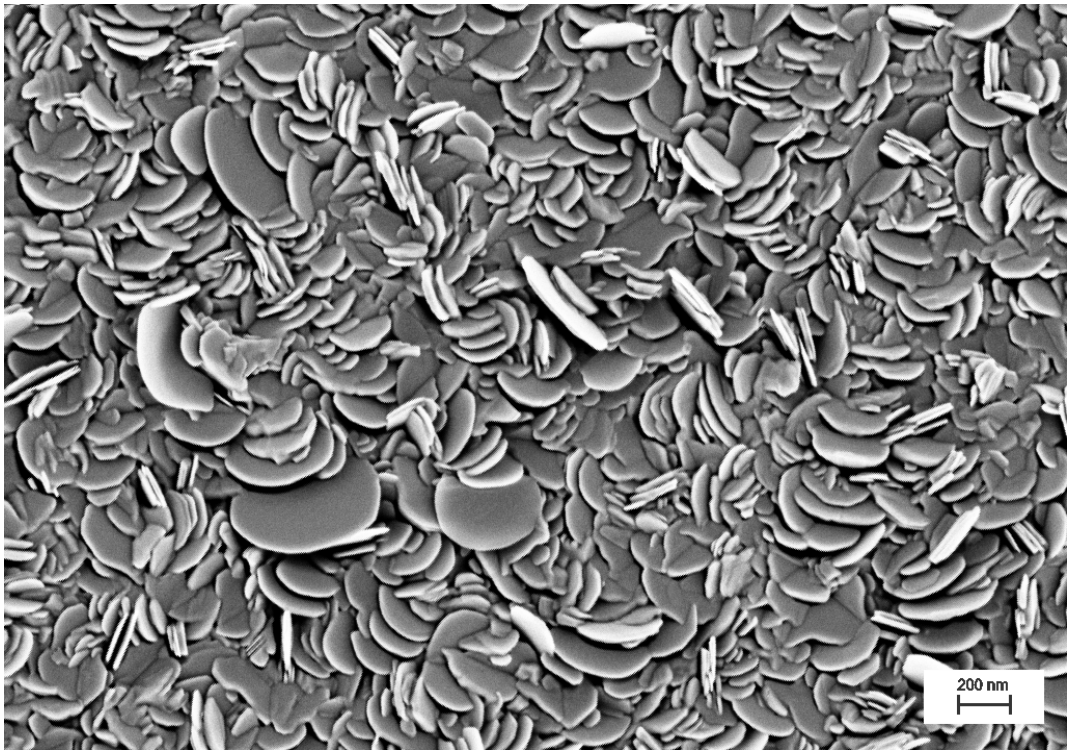


c)

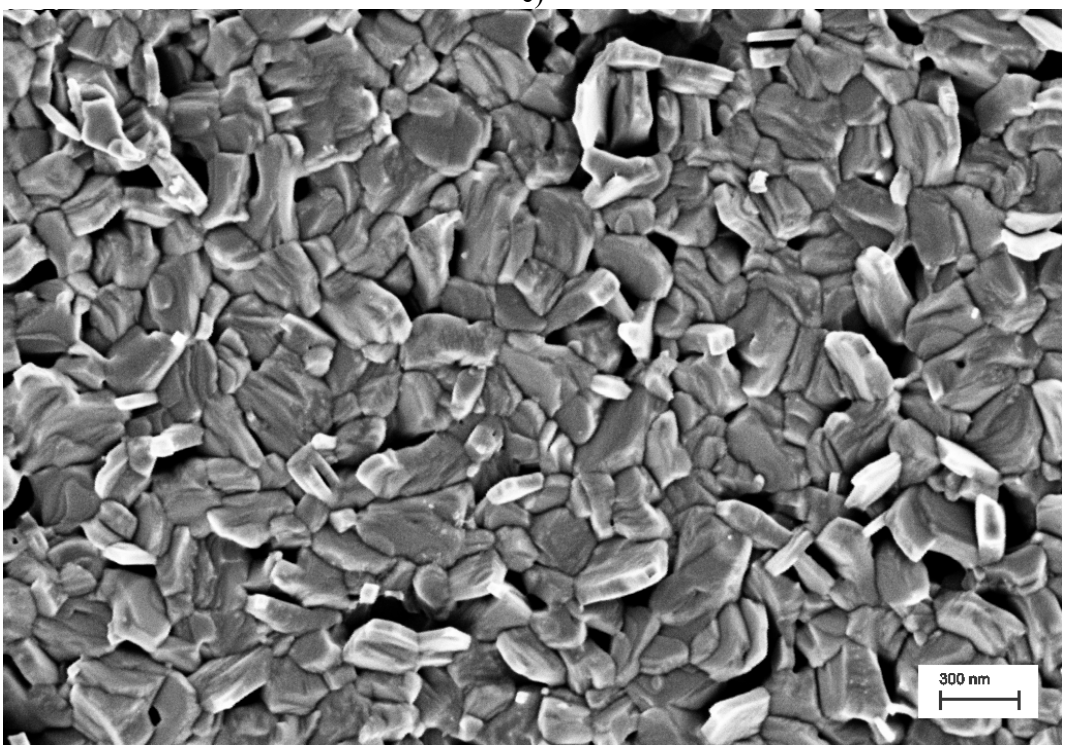


d)

*Figure 5: HR-SEM surface images of: (a) as-deposited SnS film ,and vacuum annealed SnS films at (b) 300 ºC, (c) 450 ºC, (d) 500 ºC.*

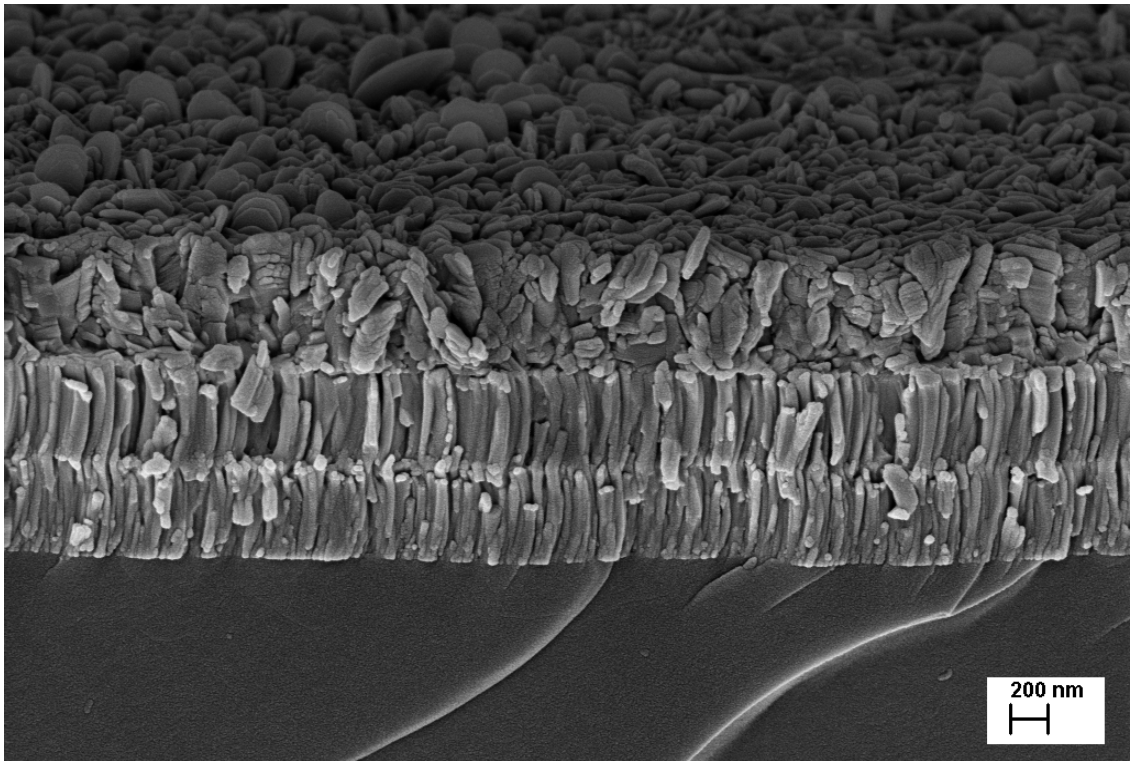


a)

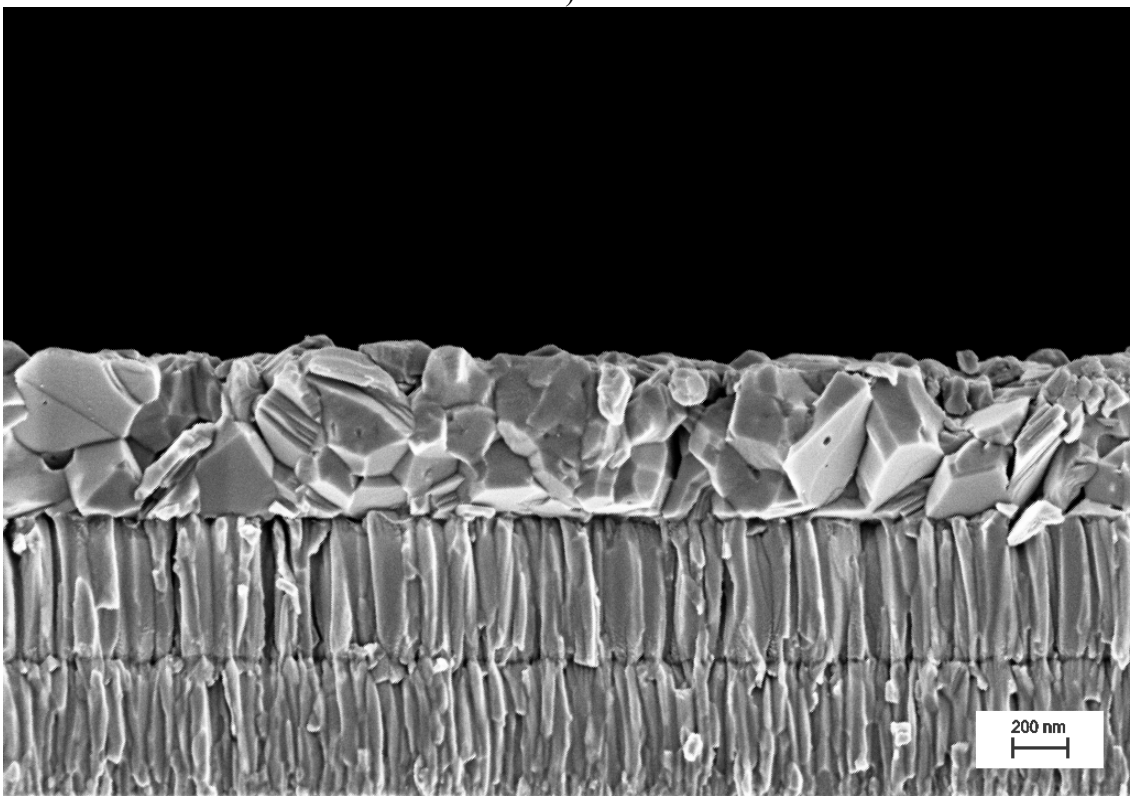


b)

*Figure 6: HR-SEM cross sectional images of glass/Mo/SnS structures: (a) as-deposited and (b) annealed at 500 ºC.*

### *3.2 Structural Properties*

The XRD profiles of as-deposited and vacuum annealed SnS films are shown in *Figure 7*. The XRD measurements revealed that all samples exhibit polycrystalline nature. Both as-deposited and annealed films showed crystallites with preferred orientation of (040) along with other directions of (120), (131), (151) planes that corresponds to orthorhombic crystal structure of SnS with no additional phases in it. The XRD peak positions are indexed using the JCPDS database (Card № 39-0354). With increase of annealing temperature, the intensity of (040) plane increases and becomes more intense and sharper that indicates improvement in the crystalline quality of the layers.

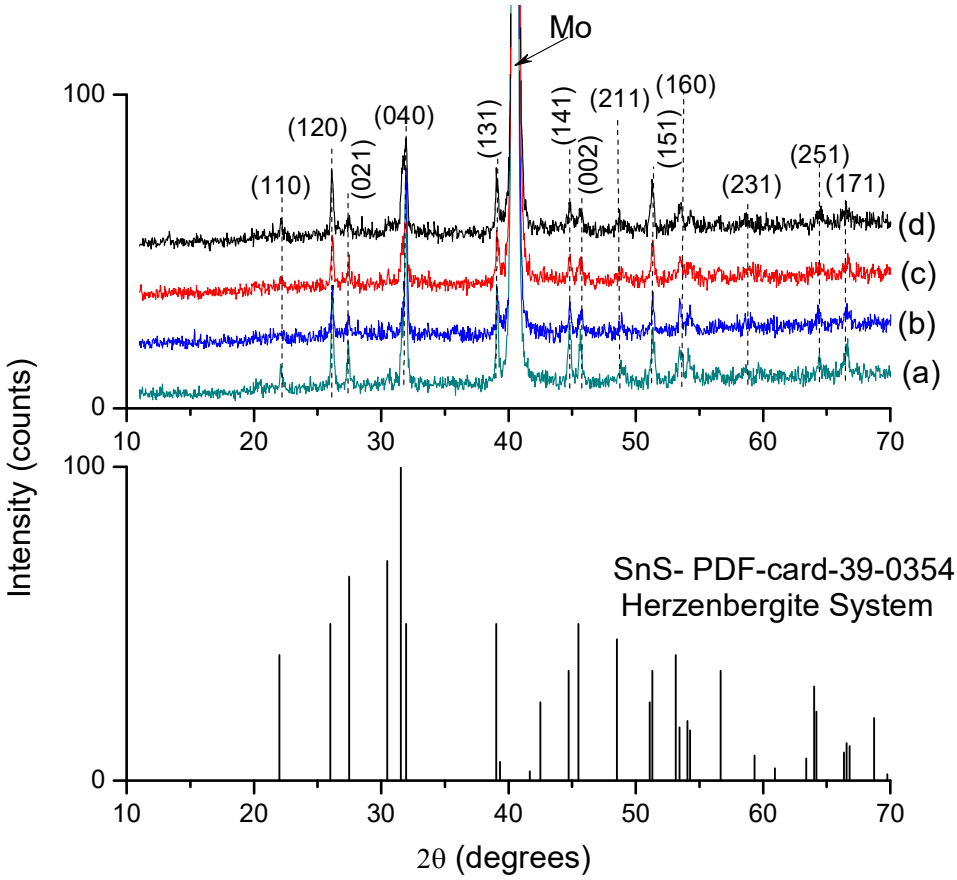


*Figure 7: XRD patterns of (a) as-deposited and vacuum annealed at (b) 300 ºC, (c) 450 ºC and (d) 500 ºC SnS films.*

The XRD patterns indicate good crystallinity and large grain sizes due to the narrow peak width. The average crystallite size was estimated using the Debye-Scherrer formula (3.1) with full width at half maximum of the (040) plane and is shown in Table 2. The calculated average crystallite size increased from 17.6 nm for as-deposited films to 55.2 nm for the films

annealed at 500 ºC. The observed increase in average crystallite with annealing is due to the improvement in crystallinity in which the atoms occupied minimum energy positions and hence helps for the rearrangement and recrystallization as a result of coalescence.

Table 2: Average crystallite sizes in vacuum annealed SnS films.

| Sample condition | Size (nm) |
|---|---|
| As-deposited | 17.6 |
| Annealed at 300 ºC | 28.4 |
| Annealed at 450 ºC | 48.6 |
| Annealed at 500 ºC | 55.2 |

From the XRD pattern, the lattice constants for the orthorhombic SnS were calculated using the equation (3.3). The evaluated lattice parameters for as deposited film was found to be a = 4.30 Å, b = 11.19 Å and c = 4.01 Å, respectively, while the annealed films showed similar results. These results are in a good agreement with data for bulk SnS [76] and SnS thin films [77]. This infers that there is no changes in the diffraction peak position for as-deposited and annealed films, which could be attributed to the strain free films with good structural quality.

## *3.3 Raman Analysis*

*Figure 8* shows Raman spectra of as-deposited and annealed SnS films. Raman analysis confirms the single phase composition of orthorhombic SnS for as-deposited and annealed layers without visible traces of any secondary phases like $SnS_2$, $Sn_2S_3$ etc. Raman spectra showed vibrational peaks at 95, 160, 190 and 218 $cm^{-1}$ of SnS.

The unit cell of SnS belongs to the $D_{2h}^{16}$ space group [78]. The factor-group analyses disclose 24 vibrational modes - 21 optical and 3 acoustic phonons ($1B_{1u}$, $1B_{3u}$, $1B_{2u}$) forming the irreducible representation at the centre of Brillouin Zone [78]:

$$\Gamma_{SnS}=4A_g+4B_{2g}+4B_{1u}+4B_{3u}+2A_u+2B_{1g}+2B_{3g}+2B_{2u} \quad (4.1)$$

from which 2 are inactive ($2A_u$), 7 are infrared active ($3B_{1u}$, $3B_{3u}$, $1B_{2u}$) and 12 are Raman active ($4A_g$, $2B_{1g}$, $4B_{2g}$, $2B_{3g}$).

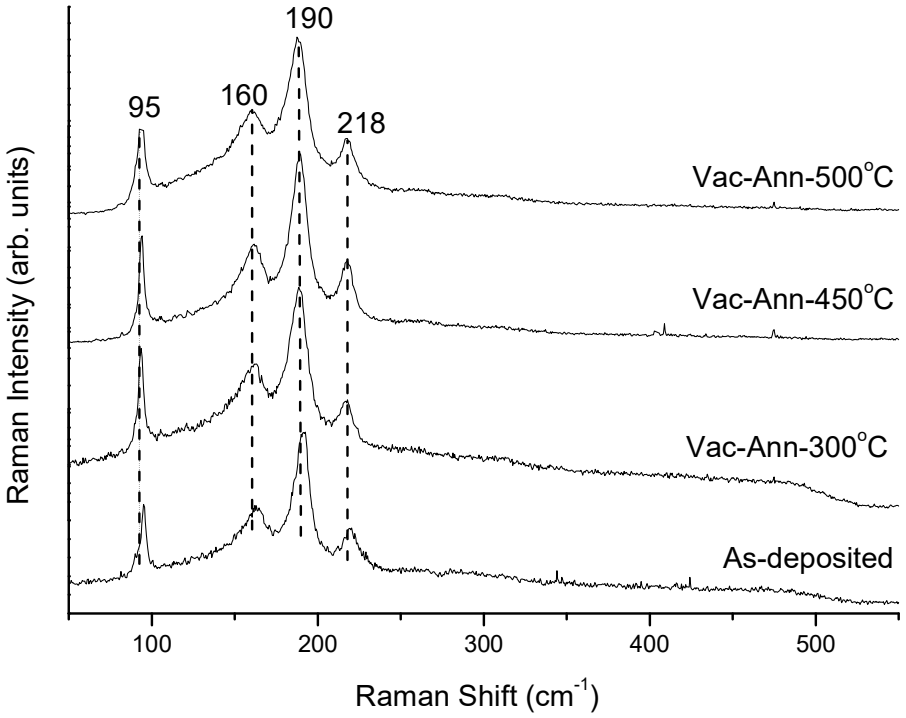


*Figure 8: Raman Spectra of as-deposited and vacuum annealed samples.*

Obtained peaks are in a good agreement with reported papers [79, 80]. The peaks obtained at 95, 190 and 218 $cm^{-1}$ corresponds to $A_g$ vibrational mode, whereas 160 $cm^{-1}$ corresponds to $B_{2g}$ vibrational mode [80]. According to Mulliken symbol definition, $A_g$ mode is one dimensional, symmetric vibration and $B_{2g}$ is a one dimensional, anti-symmetric vibration with respect to principal axis [81]. $A_g$ mode in SnS is a shear mode along the $\bar{a}$ direction [80] and the incident beam and scattered beam as well as polarization vectors of the incident and scattered photons are parallel to each other and are along the $\bar{c}$ and $\bar{a}$ directions, respectively. $B_{2g}$ in SnS is a compressive mode of vibration along the $\bar{c}$ direction. In this mode, directions of incident and scattered laser beams are parallel and are along the $\bar{b}$ direction, whereas the polarization vectors of the incident and scattered photons form 90º and are along the $\bar{a}$ and $\bar{c}$ directions, respectively [80]. From the incident and scattered beam directions, it can be assumed that all 4 peaks represent longitudinal modes of vibration. Also, it can be seen from *Figure 8*, that peaks corresponding to $A_g$ modes have higher intensity than peak corresponding to $B_{2g}$ mode. This can be because of difference in concentrations of active groups or due to the fact that the scales are not the same in different directions.

### *3.4 Optical Studies*

The optical transmittance and reflectance measurements were recorded in the 300 – 1500 nm wavelength range for the as-deposited and annealed SnS films and are shown in *Figure 9a*. As it can be seen from the *Figure 9a*, in the visible range of the spectra the reflectance is between 20-30 % for all films, whereas the transmittance is practically 0%. The fundamental absorption edge was found to be at around 950-1000 nm, above which all the curves exhibit oscillatory behavior, which might be a result of interference phenomena between two surfaces of the SnS film [84]. The sums of transmittance and reflectance curves versus the wavelength for as-deposited and vacuum annealed films are illustrated in *Figure 9b*. As it can be observed from the *Figure 9b*, the sum of transmittance and reflectance is very high in the infrared region of spectra that increases with increasing wavelength and approaches close to 100 % at 1500 nm, while the sum of transmittance and reflectance is around 15-25 % in the visible region of the spectra, which means that the rest of the light – 75-85 % is absorbed by the SnS films, thus confirming the high absorption coefficient of the films. The absorption coefficient was estimated from transmittance and reflectance data using equation (3.4), and is found to be in order of $10^5$ $cm^{-1}$ for all the films at the fundamental absorption edge, that is in a good agreement with literary data [37, 46, 50, 69].

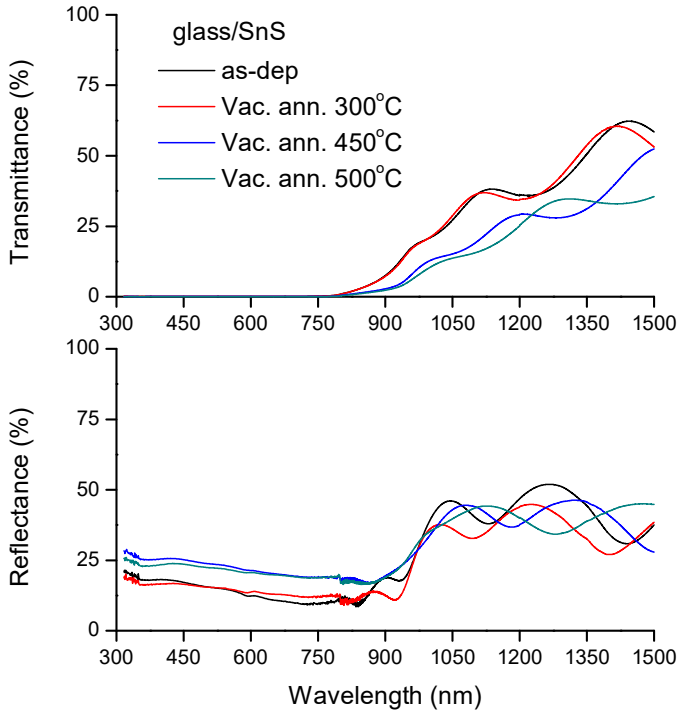


a)

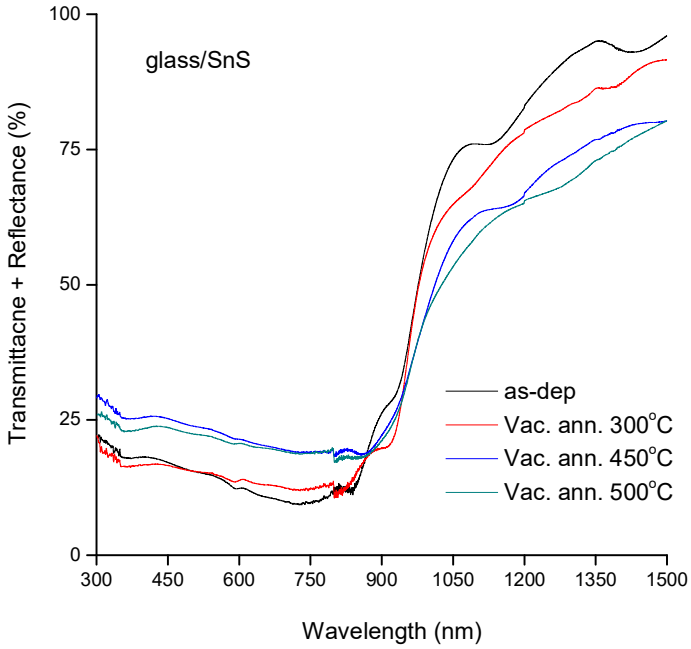


b)

*Figure 9: (a) Transmittance, Reflectance and (b) Transmittance + Reflectance spectra of the vacuumed annealed films.*

In the present study, the nature of the optical transition in SnS was found to be direct and the energy band gap was estimated by extrapolating the linear portion on to energy (hν) axis and taking the intercept (see section 3.4). The optical band gaps of as-deposited and vacuum-annealed films are shown in *Figure 10*. As it can be seen from the figure, the band gap of as-deposited SnS film is 1.5 eV, which further decreases to 1.4 eV with increasing annealing temperature to 500 ºC. This small change in band gap as a function of annealing temperature might be due to improvement in the crystallinity size of the films [85]. The obtained values of the band gaps are in a good match with published data for thermally evaporated and annealed SnS films [33, 37, 52, 55].

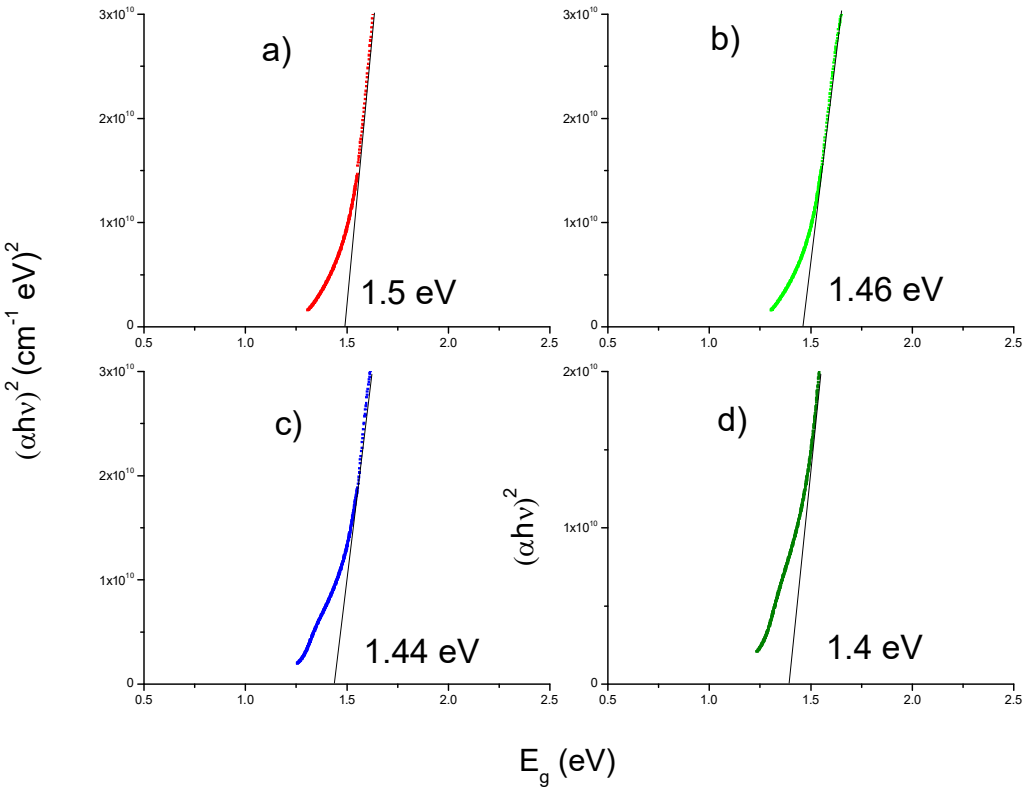


*Figure 10: Tauc's plots for as-deposited (a), and vacuum-annealed at 300 ºC (b), 450 ºC (c), 500 ºC (d) SnS films.*

## *3.5 Electrical Resistivity and Photoelectrochemical Measurements*

The electrical resistivity of the films was measured by Van der Pauw method using Indium as contacts. As it can be seen from the Table 3, the resistivity values decrease from 80 to 24 Ωcm with increasing annealing temperature, which are comparable and have similar tendency with earlier reported values [33, 38, 43, 70]. The decrease in resistivity with increasing annealing temperature might be due to the increase in average crystallite size and packing density as well due to overall improvement in the quality of the films, which is in agreement with the XRD and SEM results.

*Figure 11* shows photoresponse measurements of as-deposited and vacuum annealed SnS films in a three-electrode photoelectrochemical cell. As it can be seen from the *Figure 11*, all films are photosensitive, and due to light absorption electron-hole pairs are generated. The photogenerated minority carriers are transferred to the surface of the films where they

Table 3: Resistivity values for SnS films

| Sample condition | Resistivity (Ωcm) |
|---|---|
| As-deposited | 80 |
| Annealed at 300 ºC | 62 |
| Annealed at 450 ºC | 57 |
| Annealed at 500 ºC | 24 |

participate in the photoelectrochemical process. As it can be seen from the *Figure 11*, in the negative region of the voltage the photocurrent increases with increase of absolute value of applied voltage, which indicates that the films have p-type conductivity. As it can be observed from the *Figure 11*, the photosensitivity of as-deposited and annealed at 300 ºC SnS films are comparable, and there is an obvious increase of the photosensitivity of the films with increasing annealing temperature, with the highest photosensitivity achieved for the film annealed at 500 ºC, therefore confirming improvement of the total PV quality of the films with increasing of annealing temperature.

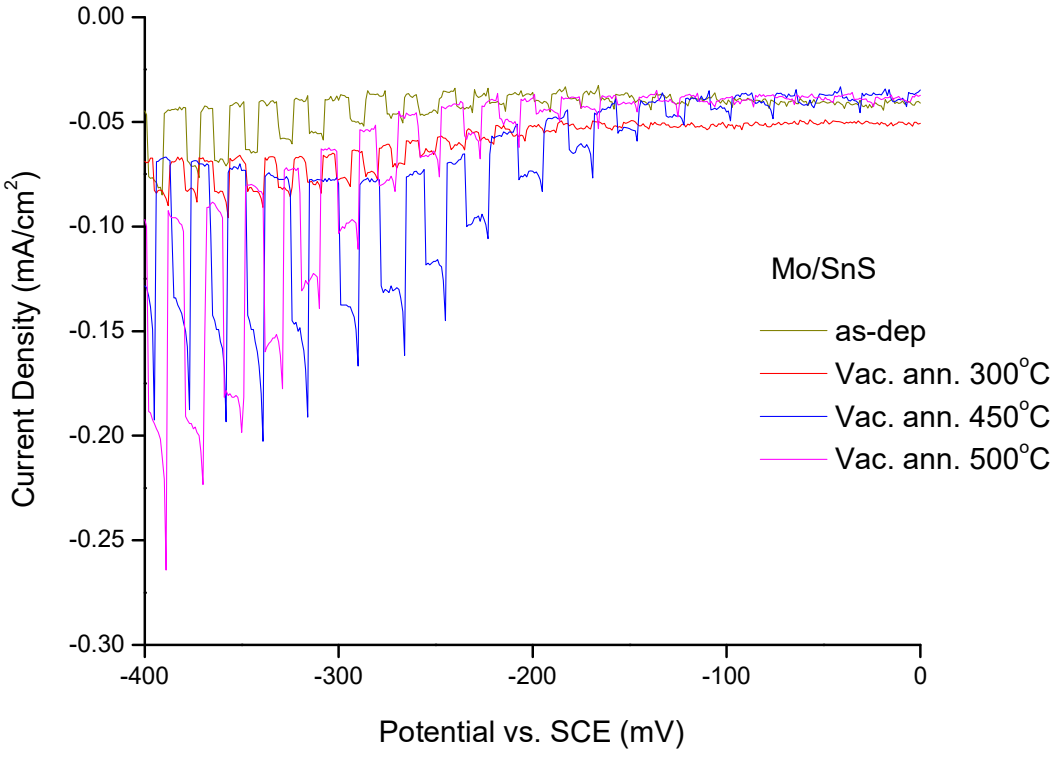


*Figure 11: Photocurrent dependence on electrode potential for glass/Mo/SnS structures in three-electrode cell in 0.1M $H_2SO_4$ background electrolyte under chopped white light illumination with 100 mW/cm$^2$ intensity.*

# Chapter 4: Conclusions

The main aim of the work was to prepare single phase composition of SnS thin films by HVE with following annealing's in vacuum ambient at different temperatures to improve the microstructural and electrical properties of as-grown SnS films. The obtained experimental results are concluded as follows:

1. Polycrystalline SnS thin films were successfully prepared by HVE method at constant deposition parameters with following annealing in vacuum at different temperatures. The obtained films were uniform, pinhole-free and well adherent to used substrate surface (SLG/Mo and SLG).

2. Annealed SnS layers didn't show any significant variations in the stoichiometric composition between Sn and S. The surface morphological studies depicts that there was changeover in shape of the grains from flakes to plate-like with more thick and dense morphology as a function of annealing temperature and also changes in grain growth from quasi 2D to 3D growth.

3. The X-ray diffraction analysis exhibits that all the layers have polycrystalline orthorhombic crystal structure of SnS with (040) as preferred plane. With increase of annealing temperature, we notice intense and sharp (040) peak that infers the improvement in crystallinity. The average crystallite size increased from 17.6 nm to 55.2 nm with increase of annealing temperature. There was no shift in the diffraction peak position, which could be attributed to the strain free films with good structural quality.

4. Raman analysis confirms the mono phase composition of SnS without any evidence of additional $SnS_2$ and $Sn_2S_3$ phases in as-deposited and annealed films. There was no changes in the peak shapes and width after annealing's.

5. The optical measurements revealed that all the layers have very high absorption coefficient around $10^5$ $cm^{-1}$ and the evaluated optical direct energy band gap was varied from 1.5 eV to 1.4 eV with increase of annealing temperature.

6. The electrical resistivity of the SnS films was found to be decreased from 80 Ωcm to 24 Ωcm with annealing's. From photoelectrochemical measurements all the layers

exhibit p-type conductivity and films annealed at 500 °C demonstrate highest photosensitivity.

The main result of this work is that high quality SnS layers produced by HVE with following annealing in vacuum at 500 °C are promising for the fabrication of complete solar cell structures based on SnS photoabsorber.

# Résumé

Being sustainable and widely available source, solar energy can be an important source for future power supplies. In the last decades, main goal of research in the PV field was development of high-efficient solar cells that consists of non-toxic, earth abundant and cost effective elements. Nowadays, most popular and widely used solar cell technology is based on monocrystalline silicon. Despite the fact that the monocrystalline silicon technology is well developed, it is still a very expensive technology. Thin film technology is an alternative technology to reduce the material utilization using direct band gap semiconductor materials with high absorption coefficient. CdTe, CIGS based solar cells are the most successful thin film solar cells. However, these cells are made of toxic Cd and expensive gallium and indium. Another emerging alternative material for thin film solar cell preparation is CZTS, which consists of less toxic and easily available elements. However, it is very difficult to control the phase composition during the synthesis and deposition process, so finding alternative materials for thin film solar cell technology is still an open challenge.

In our study we investigated tin sulfide because it is an emerging and alternative novel photoabsorber material. SnS is relatively cheap, earth abundant and environmentally acceptable compound and it is easier to control the phase composition comparing with ternary and quaternary materials. It has a high absorption coefficient (~$10^5$ $cm^{-1}$), suitable band gap (1.3-1.5 eV) and p-type conductivity. All the above mentioned properties make SnS a promising material for low-cost thin film solar cell fabrication.

In the present study, SnS thin films were deposited by high vacuum evaporation onto soda lime glass and glass/Mo substrates. Vacuum evaporation is considered to be a relatively cheap and most commonly used among physical deposition techniques for industrial production. Vacuum evaporation has some advantages e.g. deposition process done in high vacuum, which means less contamination, possibility to have high deposition rates and there is no substrate surface damage and heating since the particles have little energy.

The obtained as-deposited SnS thin films were annealed in vacuum ambient at different temperatures in sealed small quartz ampoules (closed system) to improve the crystalline quality and photoabsorber properties. Although there are number of papers on vacuum evaporation and vacuum annealing of SnS thin films, all papers describe vacuum annealing in an open system (vacuum chamber and/ or quartz process tubes), while annealing in closed system is not investigated yet.

In order to evaluate properties of as grown and vacuum annealed layers, SnS thin films were characterized and analyzed by various techniques. All the layers show nearly stoichiometric composition. The improvement in grain growth was observed from morphological analysis after annealing's. XRD and Raman studies revealed orthorhombic crystal structure with single phase composition in all the films. Optical transmittance and reflectance studies were performed to evaluate the absorption coefficient of the films and found that value to be around $10^5$ $cm^{-1}$ and estimated optical band gap of the films decreased slightly from 1.5 eV to 1.4 eV with increase of annealing temperature. The layers showed high photosensitivity and decreasing resistivity with increasing annealing temperature. As a result, we found optimal conditions to obtain highly photosensitive SnS photoabsorber layers for potential solar cell applications.

# Kokkuvõte

Päikeseenergiat, kui säästvat ja kõigile kättesaadavat energiaallikat kasutatakse aina rohkem. Viimastel aastakümnetel on PV tehnoloogiate arengus põhitähelepanu olnud päikesepaneelide võimalikult suurele kasutegurile, nendes kasutatavate materjalide toksilisusele ja kättesaadavusele loodusest, mis oluliselt mõjutab nii valmistatavate päikesepatareide kui ka nende abil saadava energia hinda. Hetkel kõige laialdasemalt kasutatav PV tehnoloogia põhineb monokristallilisel ränil, mis on küll väga hästi uuritud seoses mikrotehnoloogia väga kiirele arengule, kuid monokristallilise räni tehnoloogia on endiselt väga kallis. Alternatiivseks tehnoloogiaks on õhukesekileline tehnoloogia, mis võimaldab vähendada kasutatavate materjalide kogust ning kasutada materjale, millel on sobilik keelutsooni laius ning kõrge päikesekiirguse neeldumiskoefitsient. CdTe ja CIGS baasil valmistatud päikesepatareid on seni küll kõige efektiivsemad õhukesekilelised päikesepatareid, kuid neis sisaldub raskemetalle nagu kaadmium ning kallid materjalid nagu gallium ja indium sunnivad teadlasi otsima uusi effektiivseid materjale päikesepaneelide valmistamiseks. Teine võimalik alternatiivne materjal, millega aktiivselt tegeletakse on nelikühend CZTSSe, mis on vähem toksiline ning koosneb loodusest kergesti kättesaadavatest elementidest. Paraku on raske kontrollida CZTSSe faasikoostist sünteesi ja sadestamisprotsessi kestel. Seega võime öelda, et efektiivsete päikesepatareide tehnoloogia väljatöötamine ja nende valmistamiseks sobivate materjalide leidmine on kõigile teadlastele endiselt suureks väljakutseks.

Meie uurisime tinasulfiidi, mida peetakse hetkel väga perspektiivseks fotoabsorbermaterjaliks. SnS esineb looduses piisavalt ja see ühend ei kujuta endast ohtu keskkonnale. Kõrge valguse neeldumiskoefitsient (~$10^5$ $cm^{-1}$), sobiv keelutsooni laius (1.3-1.5 eV), p-tüüpi juhtivus ning eeldatavalt madal tootmishind on omadused, mis teevad antud ühendi eriti perspektiivseks. Võrreldes eelpoolmainitud kolmik- ja nelikühenditega on SnS-di puhul kergem jälgida ning kontrollida saadava kile faasikoostist. Antud uurimistöös sadestati SnS õhukesed kiled kõrgvaakumis Mo-ga kaetud klaasalustele. Kasutatud vaakumaurustusmeetodit loetakse suhteliselt odavaks kuid ka efektiivseks tehnoloogiaks erinevatest materjalidest õhukeste kilede sadestamisel. Vaakuumaurustusmeetodi eeliseks loetakse ka asjaolu, et sadestus toimub kõrgvaakuumis, mis oluliselt vähendab mõju keskkonnale. Vahetult pärast sadestamist toimus sadestatud SnS kilede termotöötlus erinevatel temperatuuridel vakumeeritud kvartsampullis, mille jooksul paranesid kilede struktuur, muutusid nende kristallilised ja fotoabsorber omadused. Kirjandusest võime leida

suurt hulka artikleid, mis kirjeldavad vaakumaurustusmeetodil sadestatud kilede omadusi, kuid saadud kilede sadestamisele järgnevat termotöötlust on seni läbi viidud vaid avatud süsteemis. Kõiki, nii sadestatud kui ka järeltöödeldud kilesid, iseloomustati kasutades erinevaid analüüsi meetodeid, et leida võimalikke muutusi kilede keemilises ja faasikoostises ning kristallstruktuuris. Kõiki kilesid iseloomustas nende ligikaudu stöhhiomeetriline koostis, mis vastas tina monosulfiidile. XRD ja Raman spektroskoopilised uuringud näitasid, et kiled on ühefaasilise koostisega ja ortorombilise kristallstruktuuriga. Optilistel mõõtmistel määrati kilede neeldumiskoefitsient, mis oli ligikaudu $10^5$ $cm^{-1}$ ning kile materjali optiline keelutsooni laius, mis oli vahemikus 1.4 eV - 1.5 eV. Kõik kiled olid kõrge fototundlikkusega ja nende takistus sõltus termotöötlusel kasutatud temperatuurist.

# References


1. Annual Energy Outlook 2015 (With Projections to 2040). U.S. Energy Information Administration. April 2015. http://www.eia.gov/forecasts/aeo
2. K. Zweibel, Terawatt challenge for thin-film PV, Tech. Rep. NREL/TP-520-38350, 2005 Aug 01, 2005
3. R. Soref and B. Bennett, Electrooptical effects in silicon, IEEE Journal of Quantum Electronics, 23(1):123–129, 1987
4. First Solar achieves efficiency, durability milestones and sets 21.5% record for CdTe solar cell efficiency.http://investor.firstsolar.com/releasedetail.cfm?ReleaseID=895118 (accessed 5 February 2015)
5. http://www.pv-magazine.com/news/details/beitrag/solar-frontier-hits-223-on-cigscell_100022342/#axzz44H709jZe, 2015 (accessed 08.12.15)
6. B. A. Andersson, "Materials availability for large-scale thin-film photovoltaics, "Prog Photovoltaics Res Appl 8, 61-76 (2000)
7. K. Ito and T. Nakazawa, “Electrical and optical properties of stannite-type quaternary semiconductor thin films,” Japanese Journal of Applied Physics, vol. 27, no. 11, pp. 2094–2097, 1988
8. Zhai Y. T., Chen S. Y., Yang J. H., Xiang H. J., Gong X. G., Walsh A., Kang J. and Wei S. H., Structural diversity and electronic properties of Cu(2)SnX(3) (X = S, Se): A first-principles investigation. Physical Review B, 84 (7), 2011
9. F. Alharbi, J. D. Bass, A. Salhi, A. Alyamani, H. C. Kim, R. D. Miller, Abundant non-toxic materials for thin film solar cells : Alternative to conventional materials, Renewable Energy, Vol. 36, No. 10, 01.10.2011, p. 2753-2758
10. L. Sun, R. Haight, P. Sinsermsuksakul, S. B. Kim, H. H. Park and R. G. Gordon, Band alignment of SnS/Zn(O,S) heterojunctions in SnS thin film solar cells, Appl. Phys. Lett. 103, 181904 (2013)
11. M Devika, KTR Reddy, NK Reddy, K Ramesh, R Ganesan, ESR Gopal, KR Gunasekhar. “Microstructure Dependent Physical Properties of Evaporated Tin Sulfide Films”. J. Appl. Phys. 100; 023518 (1-7); 2006
12. Madelung O. (2004). Semiconductors: Data handbook. (3rd ed., pp. 1981-1989). Springer

13. . A. Green, K. Emery, Y. Hishikawa, W. Warta, and E. D. Dunlop, “Solar cell efficiency tables (version 43),” Progress in Photovoltaics, vol. 22, pp. 1–9, 2014
14. Dimroth F, Guter W, Schöne J, Welser E, Steiner M, Oliva E, Wekkeli A, Siefer G, Philipps SP, Bett AW,Metamorphic GaInP/GaInAs/Ge triple-junction solar cells with > 41 % efficiency. 34th IEEE Photovoltaic Specialists Conference. 2009
15. G. B. Haxel, J. B. Hedrick, G. J. Orris, Rare Earth Elements—Critical Resources for High Technology, http://pubs.usgs.gov/fs/2002/fs087-02/, 17.05.2005
16. L. A. Burton, Phase Stability and Composition of Tin Sulfide for Thin-Film Solar Cells, PhD thesis, University of Bath, October 2014
17. C. Anderson, Tin Mineral Commodity Survey, United States Geological Survey technical report, 2014
18. T. Jaing and G.A. Ozin, J. Mater. Chem. **8** (1998), p. 1099
19. P. A. Nwofe, Deposition and Characterisation of SnS Thin Films for Application in Photovoltaic Solar Cell Devices, PhD Thesis, University of Northumbria, 2013, p63
20. M. Merdan, Optical and Electrical Studies on Tin Sulfide, PhD Thesis, University of Nottingham, 1977, p17
21. W. Albers, C. Haas, H. J. Vink, and J. D. Wasscher, Investigation of SnS, J. of Appl. Phys. 32, 2220 (1961)
22. F. Ke, J. Yang, C. Liu, Q. Wang, Y. Li, J. Zhang, L. Wu, X. Zhang, Y. Han, B. Wu, Y. Ma, C. Gao, High-Pressure Electrical-Transport Properties of SnS: Experimental and Theoretical Approaches, The Journal of Physical Chemistry C 2013 117 (12), 6033-6038
23. T. Chattopadhyay, A. Werner, H.G. Von Schnering, J. Pannetier. Temperature and pressure induced phase transition in IV-VI compounds. Revue de Physique Appliquee, 1984, 19 (9), pp.807-813.
24. Greyson Eric C., Barton Jeremy E. and Odom Teri W. (2006), Tetrahedral Zinc Blende Tin Sulfide Nano- and Microcrystals. Small, 2: 368–371
25. L. A. Burton and A. Walsh, Phase Stability of the Earth-Abundant Tin Sulfides SnS, $SnS_2$, and $Sn_2S_3$, J. Phys. Chem. C 2012 116 (45), 24262-24267
26. W. Albers, C. Haas, H. J. Vink, and J. D. Wasscher, Investigation of SnS, J. of Appl. Phys. 32, 2220 (1961)
27. W. Albers, K. Schol, The p-T-x phase diagram of the system Sn-S, Phillips Res. Repts.16(4), 329 (1961)

28. J. S. Anderson and M. C. Morton. “The electrical conductivity of stannous sulphide”. In: Proceedings of the Royal Society of London. Series A. Mathematical and Physical Sciences 184 (1945), pp. 83–101
29. J. S. Anderson and M. C. Morton. “Semi-conducting Properties of Stannous Sulphide”. In: Nature 155 (1945), p. 112
30. J. S. Anderson and M. C. Morton. “Semi–conducting properties of stannous sulphide. Part II.—Thermoelectric effect”. In: Transactions of the Faraday Society 43 (1947), pp. 185–194
31. W. Albers, C. Haas, and F. van der Maesen. “The preparation and the electrical and optical properties of SnS crystals”. In: Journal of Physics and Chemistry of Solids 15 (1960), pp. 306–310
32. M. Ohring, “Materials Science of Thin Films: Deposition and Structure”, Second edition, 2002, ISBN: 0125249756
33. H. Noguchi, A. Setiyadi, H. Tanamura, T. Nagatomo, and O. Omoto. “Characterization of vacuum-evaporated tin sulfide film for solar cell materials”. Solar Energy Materials and Solar Cells 35 (1994), pp. 325–331
34. O. E. Ogah, G. Zoppi, I. Forbes, R.W. Miles, Thin films of tin sulphide for use in thin film solar cell devices, Thin Solid Films 517, 7, 2009, pp. 2485-2488
35. N. Koteeswara Reddy, Growth-Temperature Dependent Physical Properties of SnS Nanocrystalline Thin Films, ECS J. Solid State Sci. Technol. 2013 volume 2, issue 6, P259-P263
36. A Schneikart, H-J Schimper, A Klein and W Jaegermann, Efficiency limitations of thermally evaporated thin-film SnS solar cells, J. Phys. D: Appl. Phys. 46 (2013) 305109 (7pp)
37. M.M. El-Nahass, H.M. Zeyada, M.S. Aziz, N.A. El-Ghamaz, Optical properties of thermally evaporated SnS thin films, Optical Materials 20 (2002) 159–170
38. M Devika, N Koteeswara Reddy, K Ramesh, R Ganesan, KR Gunasekhar, ESR Gopal, KT Ramakrishna Reddy, Thickness effect on the physical properties of evaporated SnS films, Journal of the Electrochemical Society, 154 (2), 2007, H67-H73
39. S. Cheng, G. Conibeer, Physical properties of very thin SnS films deposited by thermal evaporation, Thin Solid Films 520 (2011) 837–841
40. S. Cheng and H. Zhang. “Influence of thickness on structural and optical properties of evaporated tin sulphide films”. In: Micro & Nano Letters, IET 6 (2011), pp. 473–475

41. P. Jain, P. Arun, Parameters influencing the optical properties of SnS thin films, Journal of Semiconductors, 34, (2013), 093004-5
42. M. S. Selim, M. E. Gouda, M. G. El-Shaarawy, A. M. Salem, and W. A. Abd El-Ghany. "Effect of thickness on optical properties of thermally evaporated SnS films". Thin Solid Films 527 (2013), 164–169
43. M Devika, N Koteeswara Reddy, K Ramesh , H R Sumana, K R Gunasekhar, E S R Gopal and K T Ramakrishna Reddy, The effect of substrate surface on the physical properties of SnS films, Semicond. Sci. Technol. 21 (2006) 1495–1501
44. N. Koteeswara Reddy, M. Devika, M. Prashantha, K. Ramesh, S. Venkatramana Reddy, Y. B. Hahn, K. R. Gunasekhar, The physical properties of SnS films grown on lattice-matched and amorphous substrates, Phys. Status Solidi A 207, No. 8, 1864–1869 (2010)
45. N. K. Reddy, K. Ramesh, R. Ganesan, K.T. Ramakrishna Reddy, K.R. Gunasekhar, E.S.R. Gopal, Synthesis and characterisation of co-evaporated tin sulphide thin films, Appl. Phys. A 83, 133–138 (2006)
46. C. Cifuentes, M. Botero, E. Romero, C. Calderon, G. Gordillo, Optical and Structural Studies on SnS Films Grown by Co-Evaporation, Brazilian Journal of Physics, vol. 36, no. 3B, September, 2006
47. W. Guang-Pu, Z. Zhi-Lin, Z. Wei-Ming, G. Xiang-Hong, C. Wei-Qun, Investigation On SnS Film By RF Sputtering For Photovoltaic Application, IEEE First World Conference on Photovoltaic Energy Conversion, Waikoloa, Hawaii. 1994, pp. 365–368.
48. K. Hartman, J.L. Johnson, M.I. Bertoni, D. Recht, M.J. Aziz, M.A. Scarpulla, T. Buonassisi. "SnS thin-films by RF sputtering at room temperature", Thin Solid Films 519 (2011), pp. 7421–7424
49. A. Stadler, H.J. Schimper, U. Brendel, D. Topa, A. Basch, H. Dittrich. "Analyzing UV/Vis/NIR spectra with the single-layer model—sputtered SnS thin films I: space–time dependencies". Thin Solid Films 519 (2011), pp. 7951–7958
50. R. E. Banai, H. Lee, M. Lewinsohn, M. A. Motyka, R. Chandrasekharan, N. J. Podraza, J. R. S. Brownson, and M. W. Horn, Investigation of the Absorption Properties of Sputtered Tin Sulfide Thin Films for Photovoltaic Applications, Photovoltaic Specialists Conference (PVSC), 2012 38th IEEE, pp. 000164-000169
51. K.T. Ramakrishna Reddy, P. Purandhara Reddy, Structural studies on SnS films grown by a two-stage process, Materials Letters 56 (2002) 108 – 111

52. K.T. Ramakrishna Reddy, P. Purandhara Reddy, P.K. Datta, R.W. Miles, “Formation of polycrystalline SnS layers by a two-step process”, Thin Solid Films, Volumes 403–404, 1 February 2002, Pages 116–119
53. F. Jiang, H. Shen, C. Gao, B. Liu, L. Lin, Z. Shen, Preparation and properties of SnS film grown by two-stage process, Applied Surface Science Volume 257, Issue 11, 15 March 2011, Pages 4901–4905
54. J. Malaquias, P.A. Fernandes, P.M.P. Salomé, A.F. da Cunha, Assessment of the potential of tin sulphide thin films prepared by sulphurization of metallic precursors as cell absorbers, Thin Solid Films 519 (2011) 7416–7420
55. M. Leach, K.T. Ramakrishna Reddy, M.V. Reddy, J.K. Tan, D.Y. Jang and R.W. Miles, Tin Sulphide Thin Films Synthesised using a Two Step Process, Energy Procedia Volume 15, 2012, Pages 371–378
56. J. Vidal, S. Lany, M. d’Avezac, A. Zunger, A. Zakutayev, J. Francis, J. Tate, Band-structure, optical properties, and defect physics of the photovoltaic semiconductor SnS, Applied Physics Letters 100, 032104 (2012)
57. F.-Y. Ran, Z. Xiao, H. Hiramatsu, H. Hosono, T. Kamiya, Growth of high-quality SnS epitaxial films by H2S flow pulsed laser deposition, Applied Physics Letters 104, 072106 (2014)
58. A. Tanuševski, D. Poelman, Optical and photoconductive properties of SnS thin films prepared by electron beam evaporation, Solar Energy Materials & Solar Cells 80 (2003) 297–303
59. S. A. Bashkirov, V. F. Gremenok, V. A. Ivanov, V. V. Lazenka, and K. Bente. “Tin sulfide thin films and Mo/p-SnS/n-CdS/ZnO heterojunctions for photovoltaic applications”. In: Thin Solid Films 520 (2012), pp. 5807–5810
60. H. Nozaki, M. Onod, M. Sekita, K. Kosuda, T. Wada, Variation of lattice dimensions in epitaxial SnS films on MgO(001), Journal of Solid State Chemistry, 01/2005; 178(1): 245-252
61. W. Wang, K.K. Leung, W.K. Fong, S.F. Wang, Y.Y. Hui, S.P. Lau, Z. Chen, L.J. Shi, C.B. Cao, and C. Surya. “Molecular beam epitaxy growth of high quality p-doped SnS van der Waals epitaxy on a graphene buffer layer”. Journal of Applied Physics 111 (2012), p. 093520
62. Y. G. Moussa, F. Guastavino, C. LIinares. “Preparation and Characterization of SnS Thin Films Obtained by Close-Spaced Vapor Transport for Solar Cell Application”. IEEE Proceedings (2000), pp. 66–68

63. J.Y. Kim and S.M. George. “Tin monosulfide thin films grown by atomic layer deposition using tin 2, 4-pentanedionate and hydrogen sulfide”. Journal of Physical Chemistry C 100 (2010), pp. 17597–17603
64. P. Sinsermsuksakul, J. Heo, W. Noh, A. S. Hock, and R. G. Gordon. “Atomic layer deposition of tin monosulfide thin films”. Advanced Energy Materials 1 (2011), pp. 1116–1125
65. M Devika, N Koteeswara Reddy, K Ramesh, K R Gunasekhar, E S R Gopal and K T Ramakrishna Reddy, Influence of annealing on physical properties of evaporated SnS films, Semicond. Sci. Technol.21 (2006) 1125–1131
66. G.H. Yue, W. Wang, L.S.Wang, X. Wang, P.X. Yan, Y. Chen, D.L. Peng, The effect of anneal temperature on physical properties of SnS films, Journal of Alloys and Compounds 474 (2009) 445–449
67. M Devika, N Koteeswara Reddy, S Venkatramana Reddy, K Ramesh, KR Gunasekhar, Influence of rapid thermal annealing (RTA) on the structural and electrical properties of SnS films, J Mater Sci: Mater Electron (2009) 20:1129–1134
68. O. E. Ogah, K. R. Reddy, G. Zoppi, I. Forbes, R. W. Miles, Annealing Studies and Electrical Properties of SnS-based Solar Cells, Thin Solid Films, Volume 519, Issue 21, 31 August 2011, Pages 7425–7428
69. H.-J. Jia, S.-Y. Cheng, X.-K. Wu, Y.-L. Yang, Effect of anneal temperature on electrical and optical properties of SnS:Ag thin films, Natural Science, Vol.2, No.3, 197-200 (2010)
70. M. Devika, N. Koteeswara Reddy, K.R. Gunasekhar, Structural, electrical, and optical properties of as-grown and heat treated ultra-thin SnS films, Thin Solid Films 520 (2011) 628–632
71. B. Ghosh, R. Bhattacharjee, P. Banerjee, S. Das, Structural and optoelectronic properties of vacuum evaporated SnS thin films annealed in argon ambient, Applied Surface Science 257 (2011) 3670–3676
72. P. Jain, P. Arun, Influence of grain size on the band-gap of annealed SnS thin films, Thin Solid Films Volume 548, 2 December 2013, Pages 241–246
73. M. Patel, I. Mukhopadhyay, A. Ray, Annealing influence over structural and optical properties of sprayed SnS thin films, Optical Materials 35 (2013) 1693–1699
74. V. Steinmann, R. Jaramillo, K. Hartman, R. Chakraborty, R. E. Brandt, J. R. Poindexter, Y. S. Lee, L. Sun, A. Polizzotti, H. H. Park, R. G. Gordon, T Buonassisi,

3.88% Efficient Tin Sulfide Solar Cells using Congruent Thermal Evaporation, Advanced Materials 26(44) (11/2014)

75. P. Sinsermsuksakul, L. Sun, S. W. Lee, H. H. Park, S. B. Kim, C. Yang, R. G. Gordon, Overcoming Efficiency Limitations of SnS-Based Solar Cells, Adv. Energy Mater. 2014, 1400496
76. Sugaki A., Kitakaze A., Kitazawa H., Sci. Rep. Tohoku Univ., 16, 199, (1985)
77. Bashkirov S., Lazenka V., Gremenok V., Bente K., Microstructure of SnS Thin Films Obtained by Hot Wall Vacuum Deposition Method, Journal of Advanced Microscopy Research, Volume 6, Number 2, May 2011, pp. 153-158(6)
78. J. D. Wiley, W. J. Buckel, and R. L. Schmidt, Infrared reflectivity and Raman scattering in GeS, Phys. Rev. B 13, 2489, 1976
79. P M Nikolic, P Mihajlovic and B Lavrencic, Splitting and coupling of lattice modes in the layer compound SnS, Journal of Physics C: Solid State Physics, 10-11, 1977
80. H. R. Chandrasekhar, R. G. Humphreys, U. Zwick, and M. Cardona, Infrared and Raman spectra of the IV-VI compounds SnS and SnSe, Phys. Rev. B 15, 2177, 1977
81. R. S. Mulliken, Report on Notation for the Spectra of Polyatomic Molecules, J. Chem. Phys., 1955, 23, 1997
82. B. D. Cullity, S. R. Stock, Elements of X-Ray Diffraction (3rd Edition), Prentice-hall, New Jersey, 2001
83. V. Saini, O. Abdulrazzaq, S. Bourdo, E. Dervishi, A. Petre, V. Gopal Bairi, T. Mustafa, L. Schnackenberg, T. Viswanathan and A. S. Biris, Structural and optoelectronic properties of P3HT-graphene composites prepared by in situ oxidative polymerization, J. Appl. Phys. 112, 054327 (2012)
84. J.C. Manifacier, M. De Murcia, J.P. Fillard, Optical and electrical properties of SnO2 thin films in relation to their stoichiometric deviation and their crystalline structure, Thin Solid Films, Volume 41, Issue 2, 1 March 1977, Pages 127-135
85. P. Jain, P. Arun, Influence of grain size on the band-gap of annealed SnS thin films, Thin Solid Films 548 (2013) 241–246